AD-A149 339 FUNDAMENTAL STUDIES OF GROWTH DOPING AND TRANSFORMATION 1/1
IN BETASSILICON C..(U) NORTH CAROLINA STATE UNIV AT
RALEIGH SCHOOL OF ENGINEERING R F DAVIS ET AL.
UNCLASSIFIED 31 AUG 84 NCSU-243-043-005 N00014-79-C-0121 F/G 7/2 NL

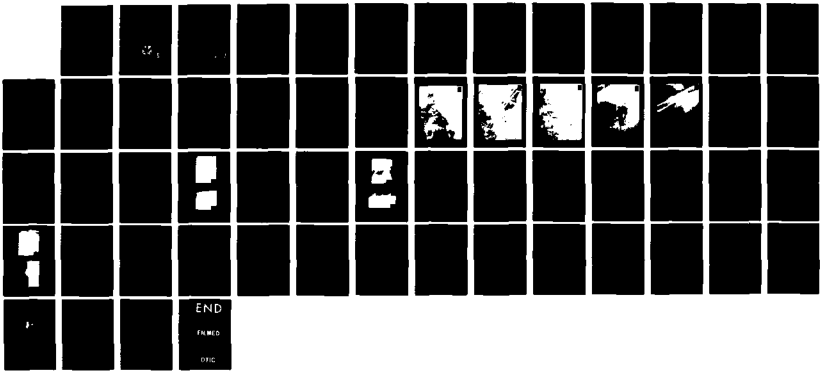

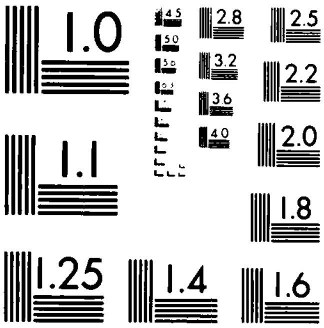

MICROCOPY RESOLUTION TEST CHART
NATIONAL BUREAU OF STANDARDS-1963-A

(14)

Annual Technical Report

FUNDAMENTAL STUDIES OF GROWTH, DOPING AND TRANSFORMATION IN BETA SILICON CARBIDE

Supported by ONR under Contract N00014-82-K-0182

For the Period September 1, 1983 - August 31, 1984

NCSU

School of Engineering
North Carolina State University
Raleigh, North Carolina

(14)

Annual Technical Report

FUNDAMENTAL STUDIES OF GROWTH, DOPING AND TRANSFORMATION IN BETA SILICON CARBIDE

Supported by ONR under Contract N00014-82-K-0182

For the Period September 1, 1983 - August 31, 1984

REPORT DOCUMENTATION PAGE

READ INSTRUCTIONS BEFORE COMPLETING FORM

1. REPORT NUMBER
243-043-005

2. GOVT ACCESSION NO.
AD-A149339

3. RECIPIENT'S CATALOG NUMBER

4. TITLE (and Subtitle)
Fundamental Studies of Growth, Doping and Transformation in Beta Silicon Carbide

5. TYPE OF REPORT & PERIOD COVERED
Annual Report

6. PERFORMING ORG. REPORT NUMBER

7. AUTHOR(s)
Robert F. Davis
H. H. Stadelmaier

8. CONTRACT OR GRANT NUMBER(s)
N00014-79-C-0121

9. PERFORMING ORGANIZATION NAME AND ADDRESS

10. PROGRAM ELEMENT, PROJECT, TASK AREA & WORK UNIT NUMBERS
PE 61153N
RR 021-02-03
NR 243-027

11. CONTROLLING OFFICE NAME AND ADDRESS
ONR-427
Arlington, VA 22217

12. REPORT DATE
August 31, 1984

13. NUMBER OF PAGES
55

14. MONITORING AGENCY NAME & ADDRESS (if different from Controlling Office)
North Carolina State University
Department of Materials Engineering
229 Riddick Laboratory
Raleigh, NC 27695-7907

15. SECURITY CLASS. (of this report)
Unclassified

15a. DECLASSIFICATION/DOWNGRADING SCHEDULE

16. DISTRIBUTION STATEMENT (of this Report)
Approved for public release; distribution unlimited

17. DISTRIBUTION STATEMENT (of the abstract entered in Block 20, if different from Report)

18. SUPPLEMENTARY NOTES
ONR Scientific Officer; Tel: (202) 696-4218

19. KEY WORDS (Continue on reverse side if necessary and identify by block number)

Silicon Carbide
Crystal Growth
Vapor Phase Epitaxy
In situ doping
Ion Implantation
Annealing
Ion Microanalysis
Oxidation
Plasma Etching
Device Preparation
Electrical Properties

Silicon carbide

20. ABSTRACT (Continue on reverse side if necessary and identify by block number)

The dopants of B, P, N, and Al have been added to CVD grown β-SiC thin films during growth and via ion implantation. A thermodynamic study has also been pursued to determine the gas phases and their partial pressures in equilibrium with the SiH_4, C_2H_4 and H_2 used to deposit the SiC. Annealing studies have shown that very high temperatures (>1750°C) are necessary to activate the implanted species. Oxidation studies, plasma etching, electrical property measurements and device fabrication have also been conducted.

DD FORM 1 JAN 73 1473 EDITION OF 1 NOV 65 IS OBSOLETE
S/N 0102-014-6601

Enclosure (1)

I. INTRODUCTION

Silicon carbide is the only compound species that exists in the solid state in the Si-C system and can occur in the cubic (C), hexagonal (H) or rhombohedral (R) structures. It is also classified as existing in the beta and alpha modifications. The beta, or cubic, form crystallizes in the zincblende or sphalerite structure; whereas, a large number (approximately 140) of the alpha occur in the hexagonal or rhombohedral forms known as polytypes.

Because of the emerging need for high temperature, high frequency and high power electric devices, blue L.E.D.'s, Schottky diodes, U. V. radiation detectors, high temperature photocells and heterojunction devices, silicon carbide is being examined throughout the world for employment as a candidate material in these specialized applications. The electron Hall mobility of high purity undoped β-SiC has been postulated from theoretical calculations to be greater than that of the α-forms over the temperature range of 300-1000K because of the smaller amount of phonon scattering in the cubic material. The energy gap is also less in the β-form (2.3 eV) compared to the α-forms (e.g., 6H = 2.86 eV). Thus, the β-form is now considered more desirable for electronic device applications, and, therefore, improvements in the growth and the characterization of thin films of this material constitute principal and ongoing objectives of this research program.

Under the previous grant, a method for the growth of single crystal thin films of β-SiC on (100) Si was developed using specially designed and very closely controlled variable pressure equipment and a two-step process. This method entails the initial chemical conversion of the Si surface via a high temperature reaction with ethylene (C_2H_4). This step is followed by direct and continual deposition of β-SiC via the separate decomposition of SiH_4 and C_2H_4 on the converted layer. H_2 is the carrier gas in both processes. Additional related research thrusts which have been conducted since that time include computer assisted calculations of CVD phase diagrams in the Si-C system, investigation of the physicochemical nature of the converted layer, ion implantation and annealing studies, electrical measurements and development of simple devices.

The specific topics addressed in this reporting period include "in situ" doping of the films during growth, continuation of the ion implant annealing program, cross section transmission electron microscopy, oxidation of the β-SiC films, establishment of an electrical characterization laboratory and subsequent measurement and continued work on device development. All of these topics are described in the succeeding sections.

In order to keep the cost and time involved in the preparation of this report and the size of the report to manageable dimensions, only the results and discussion of the research conducted from March 1-August 31, 1984 are included. The reader is referred to the report for the interval September 1, 1983-February 28, 1984 for in-depth discussions of research conducted during that period.

II. DOPING OF BETA-SiC THIN FILMS DURING GROWTH

A. Introduction

During this reporting period one of the principal objectives of this research program has been the attempt to incorporate B or Al and P or N as p- and n-type dopants, respectively, in order to produce simple discrete devices and initial samples for the future study concerning the effect of dopants on the formation of stacking faults and polytypism. Theoretical considerations of this incorporation have also been conducted in this period.

The technique of in situ doping during thin film growth contrasts with other process technologies which consist of introducing the electronically active impurities from the surface either by diffusion or by ion implantation. The former is subject to the mathematical laws of error function distribution while the latter is subject to the laws of Gaussian distribution. Thus, these processes are reasonably well-defined. It is also important to understand the mechanisms of incorporation of impurities during growth of a SiC layer.

A limited number of studies have been conducted to investigate the incorporation of impurities in β-SiC using CVD techniques. Bartlett,[1] Long[2] and Nishino[3] obtained p-type β-SiC by adding B_2H_6 or $AlCl_3$ during the β-SiC growth, while n-type β-SiC was produced without doping. Muench[4] doped polycrystalline β-SiC by adding trimethylaluminum (TMA) to the solution used for bulk crystal growth via the Van Arkel process. Through these doping processes have been successful, the operative mechanism(s) of incorporation of these dopants have not been determined.

One or more of the mechanisms suggested for dopant incorporation in Si may also be applicable to SiC. Theories have been developed to explain the gas phase doping mechanism at low concentration levels on the basis of (1) diffusion-controlled deposition kinetics (proposed by W. H. Sheperd[5]) and (2) the equilibrium solubility mechanism (proposed by Reiss[6] and extended by Rai-Choudhury and Salkovitz[7]).

In the research described below, the mechanism of in situ doping during growth was investigated by initially determining the stabilities and the gas phase equilibria of the dopant gases as a function of temperature. This was followed by an experimental study of the rate of incorporation of each of the dopants as a function of the dopant concentration in the gas phase. The experimental procedures and results and discussion of this research are presented in the following sections.

B. Experimental

In this study the dopant substances are presently incorporated directly in the primary gas stream which contains SiH_4, C_2H_4 and H_2 for the chemical vapor deposition of β-SiC. The dopant hydride gases of PH_3, B_2H_6 and NH_3 contained in H_2 are employed as sources of P, B and N, respectively. Finally, liquid trimethylaluminum (TMA) has been chosen as the Al source. The concentration of this last constituent in the gas stream is altered by changing the flow rate of H_2 over the TMA. The concentrations in H_2 of all the dopant gases currently being investigated and their respective purities are given in Table I.

Table I. Concentrations and purities of gases employed as electrically active dopants during the CVD growth of β-SiC.

Dopant Gases	Bottle Concentrations	Purity
Phosphine (PH_3)	4900 ppm (in H_2)	99.9995%(VLSI)Grade
Diborane (B_2H_6)	53.0 ppm (in H_2)	99.9995%(VLSI)Grade
	2500 ppm (in H_2)*	99.9995%(Electronic) Grade
Ammonia (NH_3)	483 ppm (in H_2)	99.9995%(Nitride) Grade
Trimethylaluminum [$(CH_3)_3Al$]	Liquid source at room temperature	99.9995%

* The higher concentration B_2H_6 in H_2 has been ordered to increase the boron concentration in β-SiC.

The introduction (or lack of it) of these dopants into the β-SiC films has been analyzed quantitatively as a function of depth using the CAMECA ion microprobe. Analyses of the dopant/Si ratios of ion implanted standards throughout the concentration range of the asymetric implant profile results in linear curves of the dopant/Si ratio versus concentration which can be used to quantitatively determine the concentration of a species in the in situ doped films of β-SiC.

C. Results and Discussion

1. Free Energies of Formation of the Dopant Gases.

Figure I shows the standard free energies of formation of the dopant gases of B_2H_6, PH_3 and NH_3 in the form of an Ellingham diagram produced from data given in the JANAF Thermochemical Tables.[8] Data for trimethylaluminum (TMA) is not available. A noteworthy feature of the diagram is that all of the dopant gases have positive free energies of formation at our experimental deposition temperature of 1633°K. Therefore, these gases might be expected to completely dissociate at the deposition temperature, if the kinetics for this process are also favorable. However, one must also consider the effect of the other gases present during CVD on the stability of these dopant sources.

2. Free Energy Minimization Calculations and the Determination of the Gas Species Present during Deposition.

Thermodynamic calculations involving all the gases present during deposition provide important information concerning the thermal stability of the dopant gases and allow an educated guess at the molecular and atomic species which are important in determining the kinetics of the CVD reaction.

Calculations of gas phase equilibria for the dopant sources were made by using the computer program "SOLGASMIX-PV" which determines equilibrium compositions by direct minimization of the total free energy of a system at various combinations of temperature, total pressure and gas composition. The necessary thermodynamic values for most of the many species which were considered to possibly exist during deposition were also taken from the JANAF Tables.[8]

The data resulting from these calculations are shown in Figs. 2, 3, and 4. These figures show the calculated equilibrium partial pressures for the various possible gaseous constituents which contain the dopant vs initial reactant gas pressure for P (Fig. 2), B (Fig. 3) and N (Fig. 4) in the Si-C-H system.

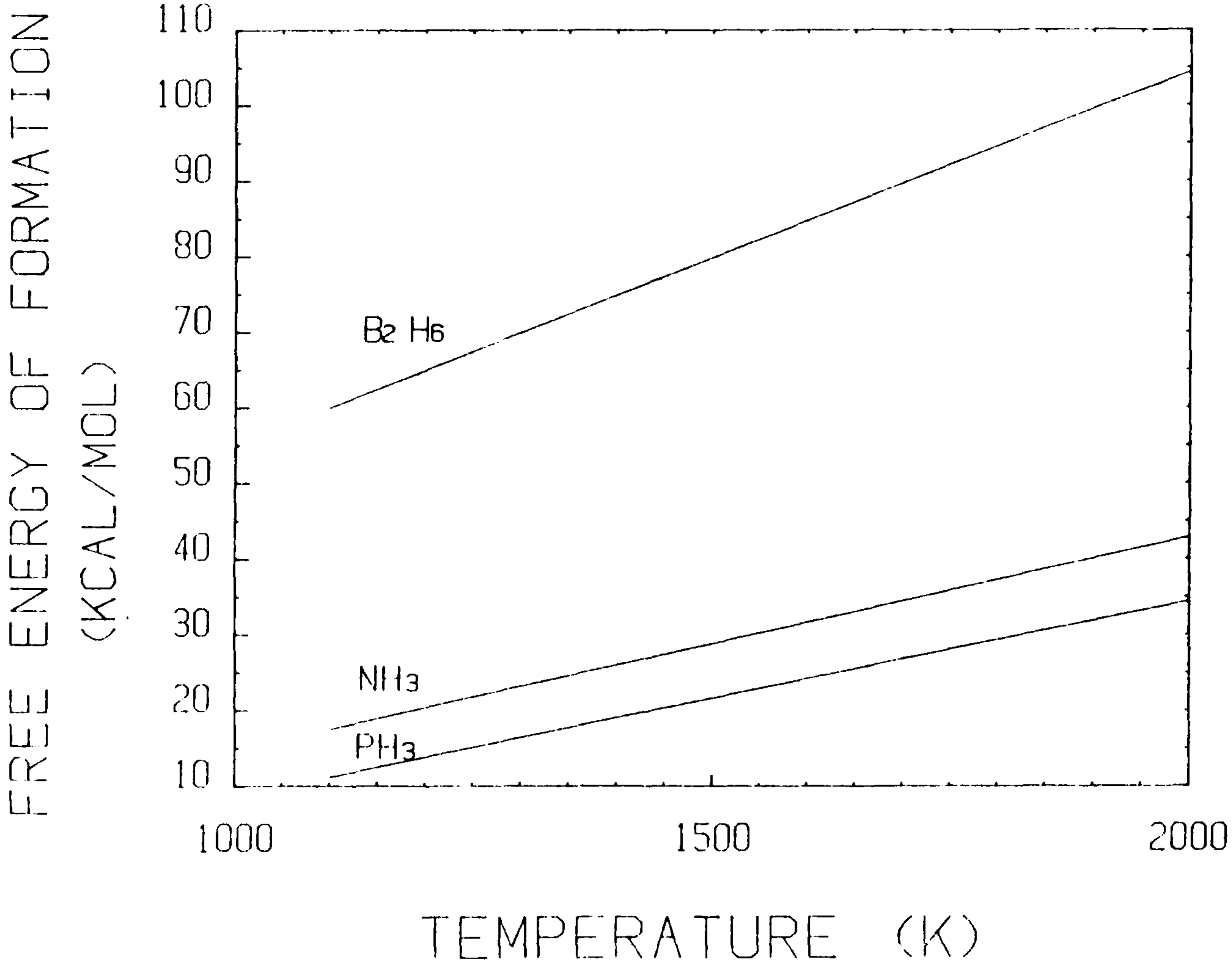

Figure 1. Free energies of formation vs temperature for B_2H_6, NH_3 and PH_3.

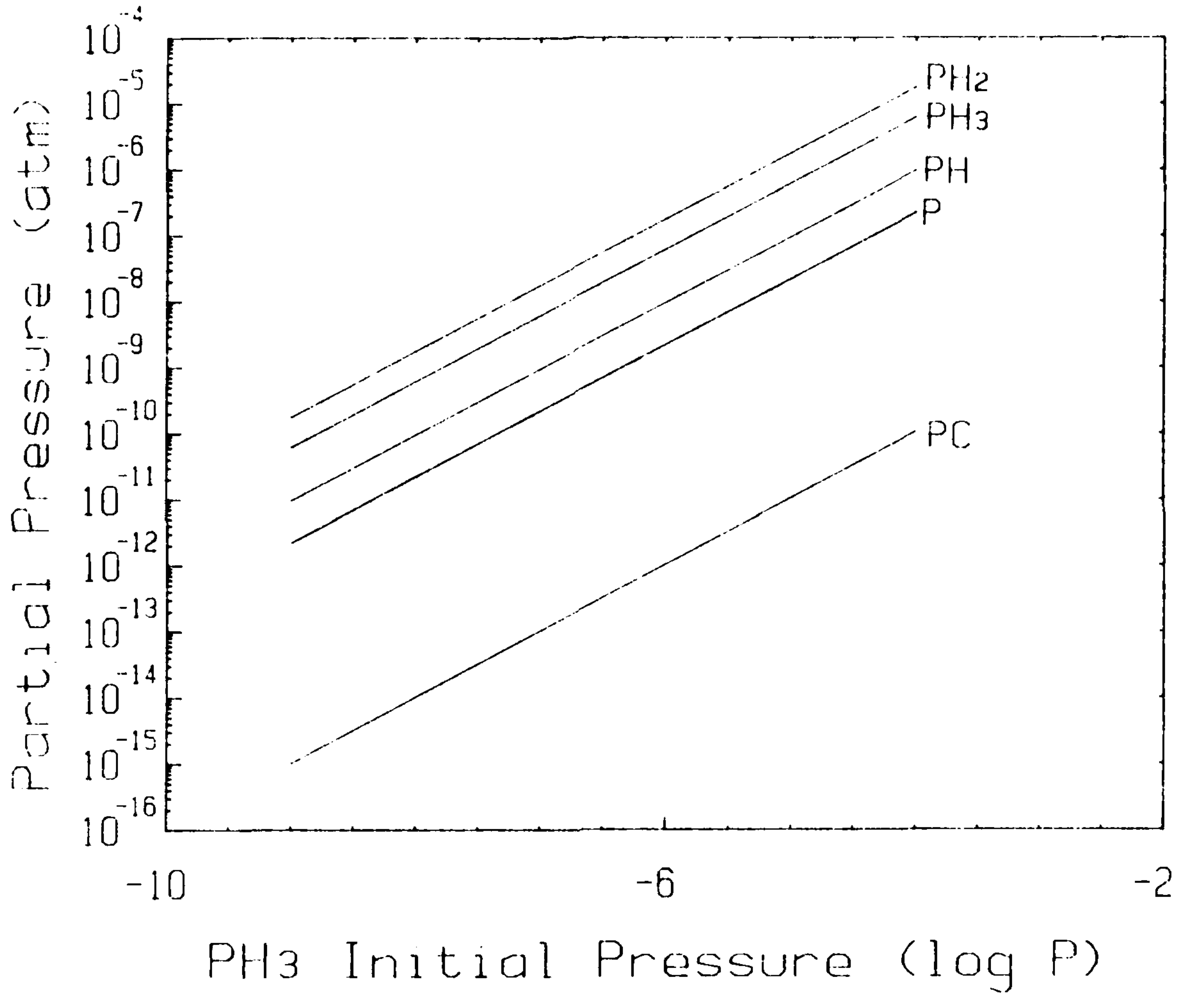

Figure 2. Calculated partial pressures of the equilibrium gas species vs the initial PH_3 gas pressure for the conditions used at NCSU in the CVD deposition of β-SiC. I.e., the gases of C_2H_4, SiH_4 and H_2 were also considered present in the mole fractions used experimentally. The total pressure was considered to be one atmosphere. PC = phosphorous carbide (gas).

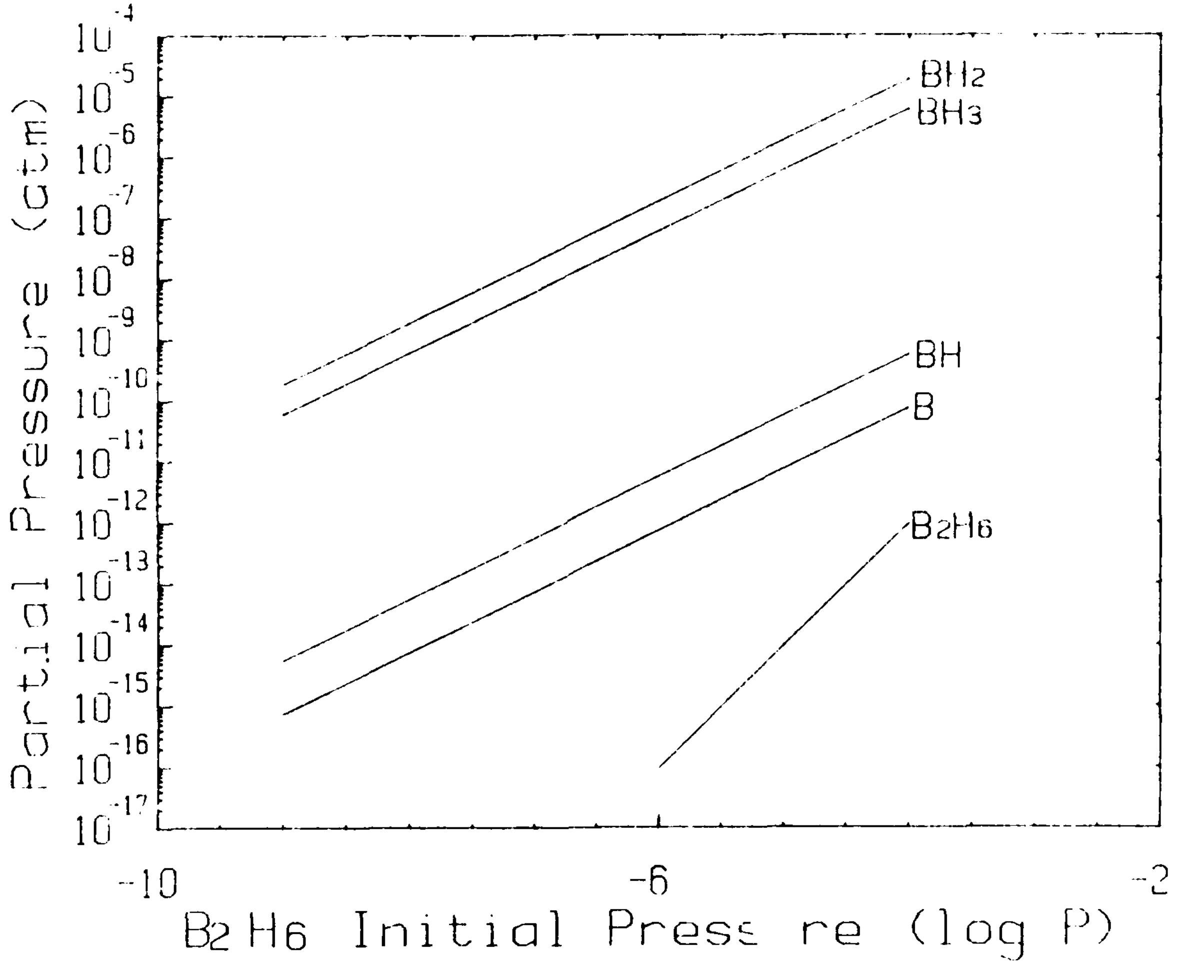

Figure 3. Calculated partial pressures of equilibrium gas species vs initial B_2H_6 gas pressure for the conditions used at NCSU in the CVD deposition of β-SiC. I.e., the gases of C_2H_4, SiH_4, and H_2 were also considered present in the mole fractions used experimentally. The total pressure was considered to be one atmosphere.

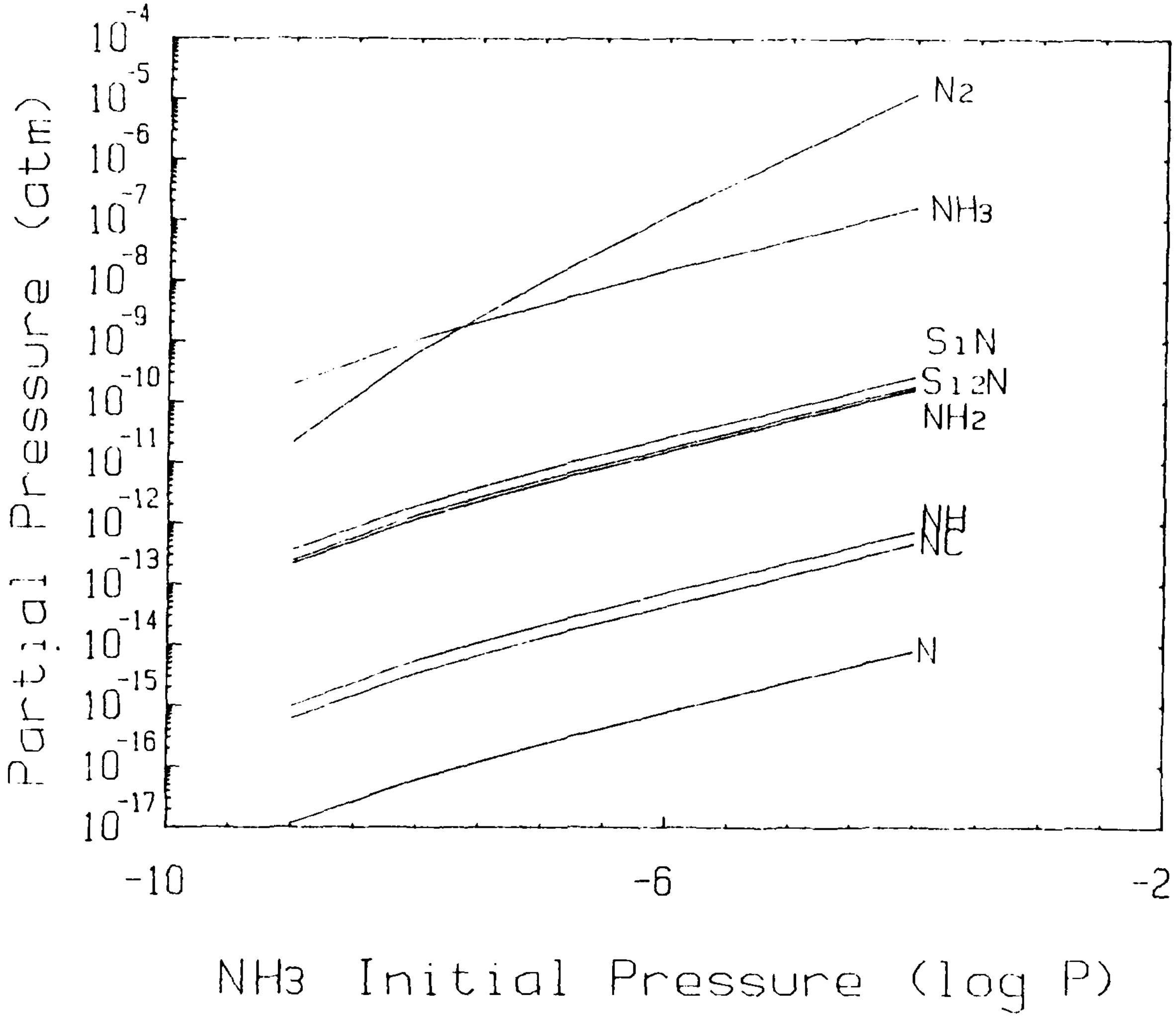

Figure 4. Calculated partial pressures of equilibrium gas species vs initial NH_3 gas pressure for the conditions used at NCSU in the CVD deposition of β-SiC. I.e., the gases of C_2H_4, SiH_4 and H_2 were also considered present in the mole fractions used experimentally. The total pressure was considered to be one atmosphere. NC = nitrogen carbide (gas).

The calculations were made for the temperature of 1633°K and one atmosphere total pressure (the deposition conditions for producing intrinsic SiC). As implied above all the gases used in the deposition of β-SiC including SiH_4, C_2H_4 and H_2 as well as the dopant gas in the mole fractions normally employed or under consideration for employment (the dopant gas) were included in the calculations.

As noted above, Figs. 2-4 show only the dopant-containing vapor species. The reason for this is that under the conditions used in the present research, no dopant-containing condensed phases were found. An interesting result provided by these calculations is that the species with the highest partial pressure at the deposition temperature are hydrides. The reason for this is the large amount of H_2 carrier gas used in the deposition process which prevents the occurrence of high concentrations of the pure elemental species.

3. Equilibrium Solubility Considerations and Measured Concentrations of Dopants in SiC Thin Films.

Using the equilibrium solubility considerations of Rai-Choudhury and Salkavitz,[7] the dopant species, when dissolved but not electrically activated (ionized) in the silicon carbide, is presumed to follow Henry's law for a dilute solute, i.e.,

$$P_D^{1/y} = K_D' N_D' \tag{1}$$

where P_D is the gas phase partial pressure of the dopant species in equilibrium with the solid; Y is the number of dopant atoms per molecule of the above species; K_D' is the Henry's law constant of the dopant in the solid solution, and N_D' is the concentration of unionized dopant in the solid solution. The activity coefficient, γ_D, may be defined as follows

$$\gamma_D = \frac{N_D' K_D'}{N_D K_D} \tag{2}$$

where γ_D is the ratio of the unionized dopant atom concentration at some actual N_D to that at infinite dilution; N_D is the total chemical concentration of the dopant and K_D is a new Henry's law constant for total dopant concentration.

Combining equations (1) and (2), one gets

$$P_D^{1/y} = K_D \gamma_D N_D \qquad (3)$$

This last equation predicts that a plot of log N_D vs log P_D should be linear with a slope 1/y, for $N_D < 1 \times 10^{18}$ cm^{-3} at typical epitaxial deposition temperatures. At higher concentrations, where a significant fraction of the donor or acceptor atoms in the solid are ionized, the activity coefficient becomes larger than one.

The above procedure allows one to relate the solid dopant partial pressure to the gas phase dopant concentration at equilibrium. Figures 5 and 6 show the results of solid-state dopant concentration vs the initial gas phase dopant partial pressure of B and P, respectively. The solid state dopant concentrations were measured using the ion microprobe. Each figure shows that the log of the solid dopant concentration is linear when plotted as a function of the log of the gas phase dopant concentration. These results are consistent with the Henry's law description of doping.

Figure 7 shows the solid-state Al concentration in SiC as a function of the partial pressure of TMA calculated from the vapor pressure of TMS, the amount of hydrogen flowing over the TMA vessel and the temperature. This result also shows that the Al concentration tracks the partial pressure of TMA as it is altered by changes of the temperature of the TMA vessel or by H_2 flow rate through the vessel or both.

The results of this latter study are consistent with the results reported by J. Bloem[9] for dopant incorporation in Si in that the rate of dopant incorporation is linearly proportional to the mole fraction (N) of the starting dopant gas in the range of mole fractions between 10^{-9} and 10^{-6}. (Because of the considerable difficulty in incorporating N from N_2 into SiC and the receipt of NH_3 just prior to this writing, time has not allowed similar studies for N using this latter source.) However, these results do not provide an indication as to which species is in equilibrium with the impurity incorporated in the solid, i.e., which particular or multiple species provided the dopant atoms which were incorporated in the β-SiC. Furthermore, we are not sure that all of the various species predicted in Figs. 2, 3 and 4 would actually

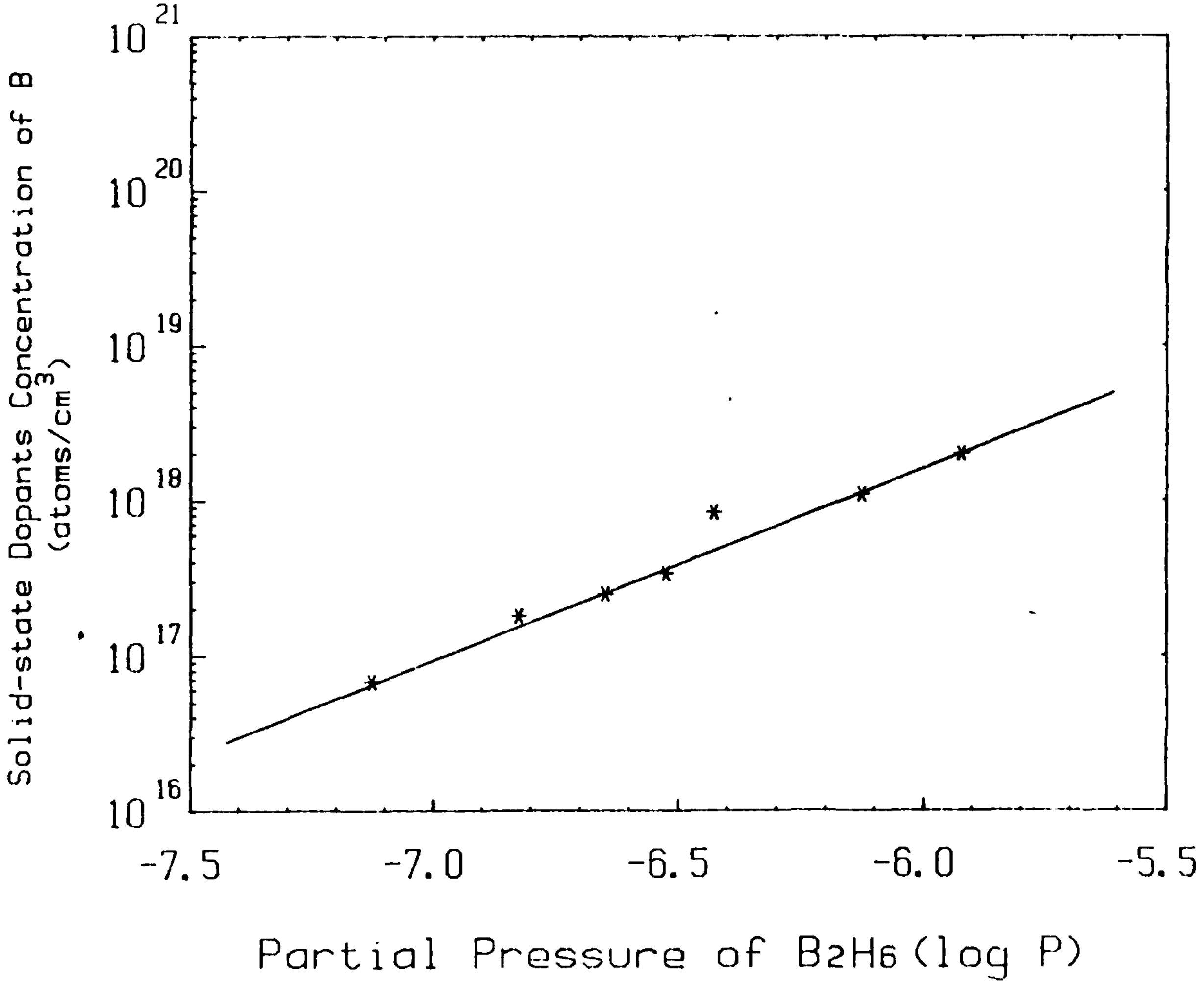

Figure 5. Experimentally measured solid-state dopant concentration of B in CVD grown β-SiC films vs initial partial pressure of B_2H_6 in flowing H_2.

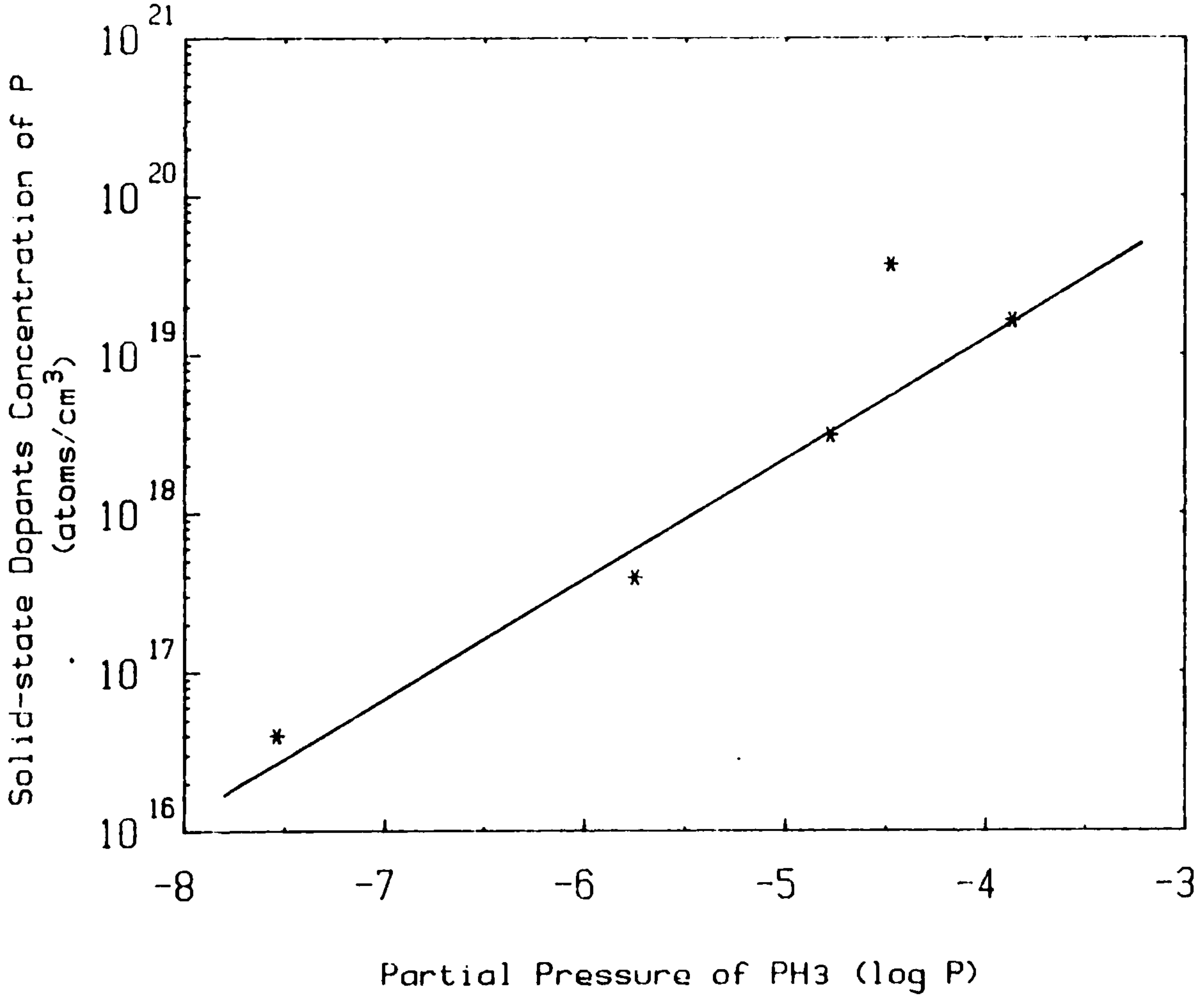

Figure 6. Experimentally measured solid-state dopant concentration of P in CVD grown β-SiC films vs initial partial pressure of PH_3 in flowing H_2.

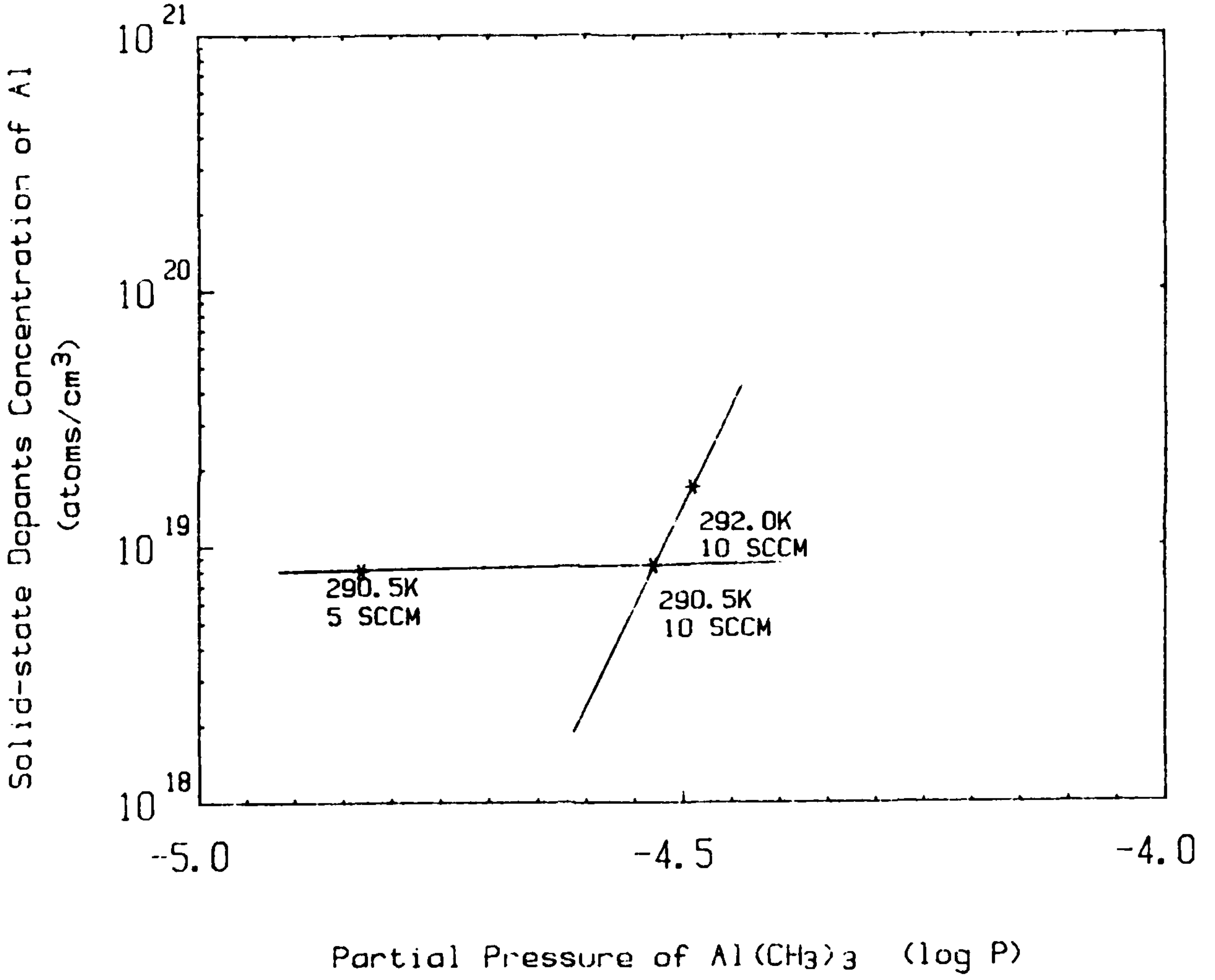

Figure 7. Experimentally measured solid-state dopant concentration of Al in the CVD β-SiC films vs initial partial pressure of $Al(CH_3)_3$ in flowing H_2.

be present in our system for it is not necessarily at equilibrium during the growth process. These calculations nevertheless provide useful insight into the dopant gas phase species which are likely to be present in equilibrium with silicon carbide and which may enter into the rate processes determining the elemental doping level in the solid thin film.

III. CROSS-SECTIONAL TRANSMISSION ELECTRON MICROSCOPY OF β-SiC FILMS

To ascertain the structural quality of the as-grown β-SiC thin films and thereby discern the efficacy of various processing parameters on the growth, we have concluded that cross-sectional transmission electron microscopy (XTEM) is the most important diagnostic tool to accomplish these objectives. This section discusses the recent findings in this area as well as provides pictorial evidence of the substructure of several of the films. The β-SiC films studied had a total thickness of approximately 11μm.

As seen in Figs. 8 ($\vec{g}$ = [111]) and 9 ($\vec{g}$ = [023]) this particular sample contains stacking faults as the major defect but also a modest concentration of dislocations--located primarily at the ends of the stacking faults (Shockley partials). A set of partials can be seen in Fig. 9 along the edge of a stacking fault between the letters A and B.

At the Si/β-SiC interface there begins a dense strain region which extends approximately 3μm into the film. Although this region can be observed at the top of Figs. 8 and 9, its character is more readily seen at high magnification (250,000X) in Fig. 10 ($\vec{g}$ = [111]). This micrograph was taken from the same interface region as Fig. 8. Most of the substructure shown in Fig. 10 is elastic strain rather than stacking faults and dislocations encountered further away from the interface.

Figure 11 ($\vec{g}$ = [011]) is particularly noteworthy, for here essentially all of the Si layer has been removed during sample preparation. Furthermore, the small band of Si remaining is much thinner than the SiC layer which occupies most of the photograph. Although stacking faults are still evident away from the interface, a large portion of the elastic strain has been relieved by the loss of the Si. Thus, although the converted layer allows one to grow a crack free β-SiC film on (100) Si, it does not alleviate the mismatches in thermal expansion and lattice parameter as much as was initially believed.

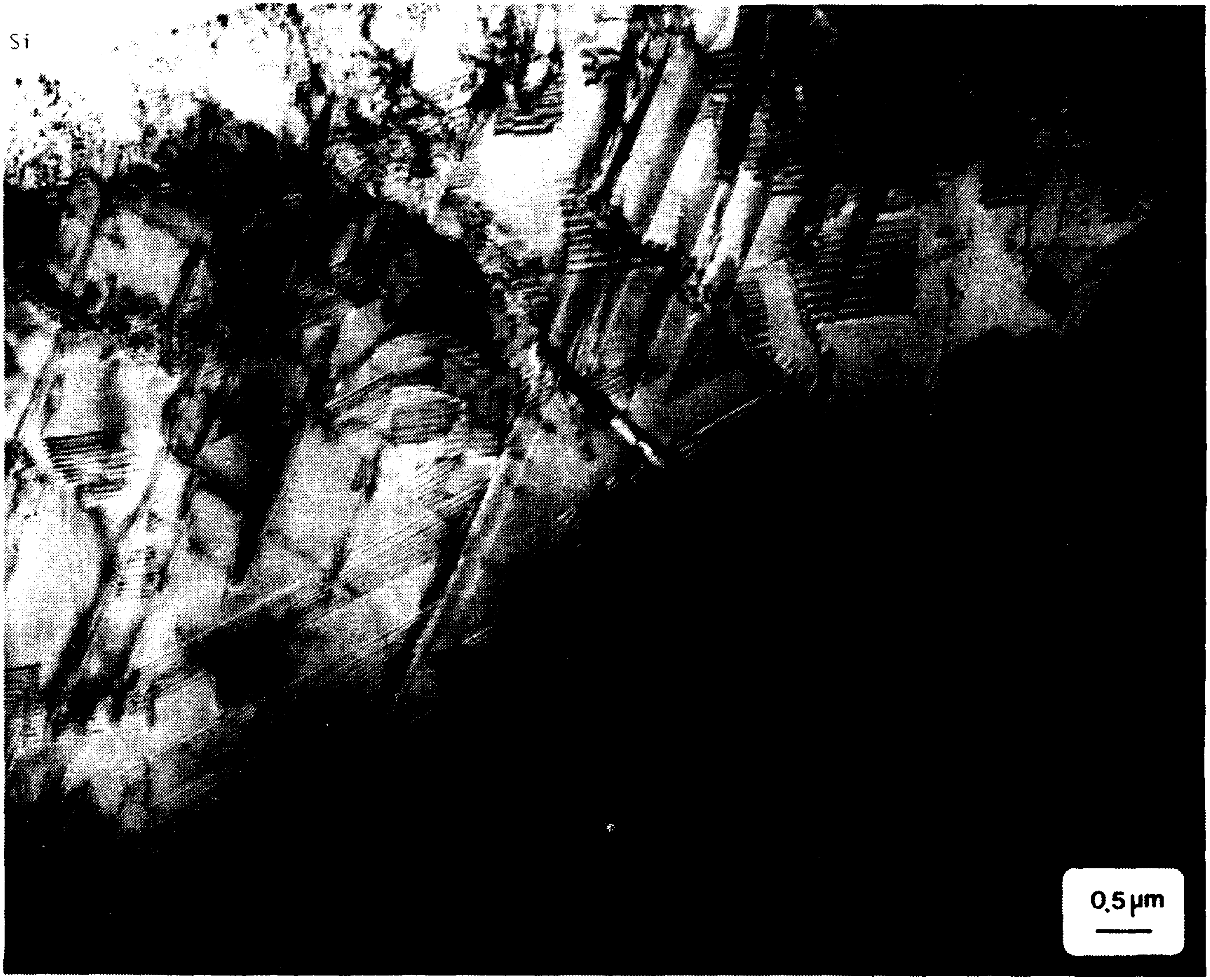

Figure 8. Cross-sectional micrographs of single crystal thin film of undoped CVD β-SiC deposited on single crystal (100) Si at 1360°C and 4 atm. using a gas mixture of SiH_4, C_2H_4 and H_2. Micrograph shows full range of defects present in the as-grown film including stacking faults, partial and misfit dislocations and interfacial strain contrast. $\vec{g}$ = [111].

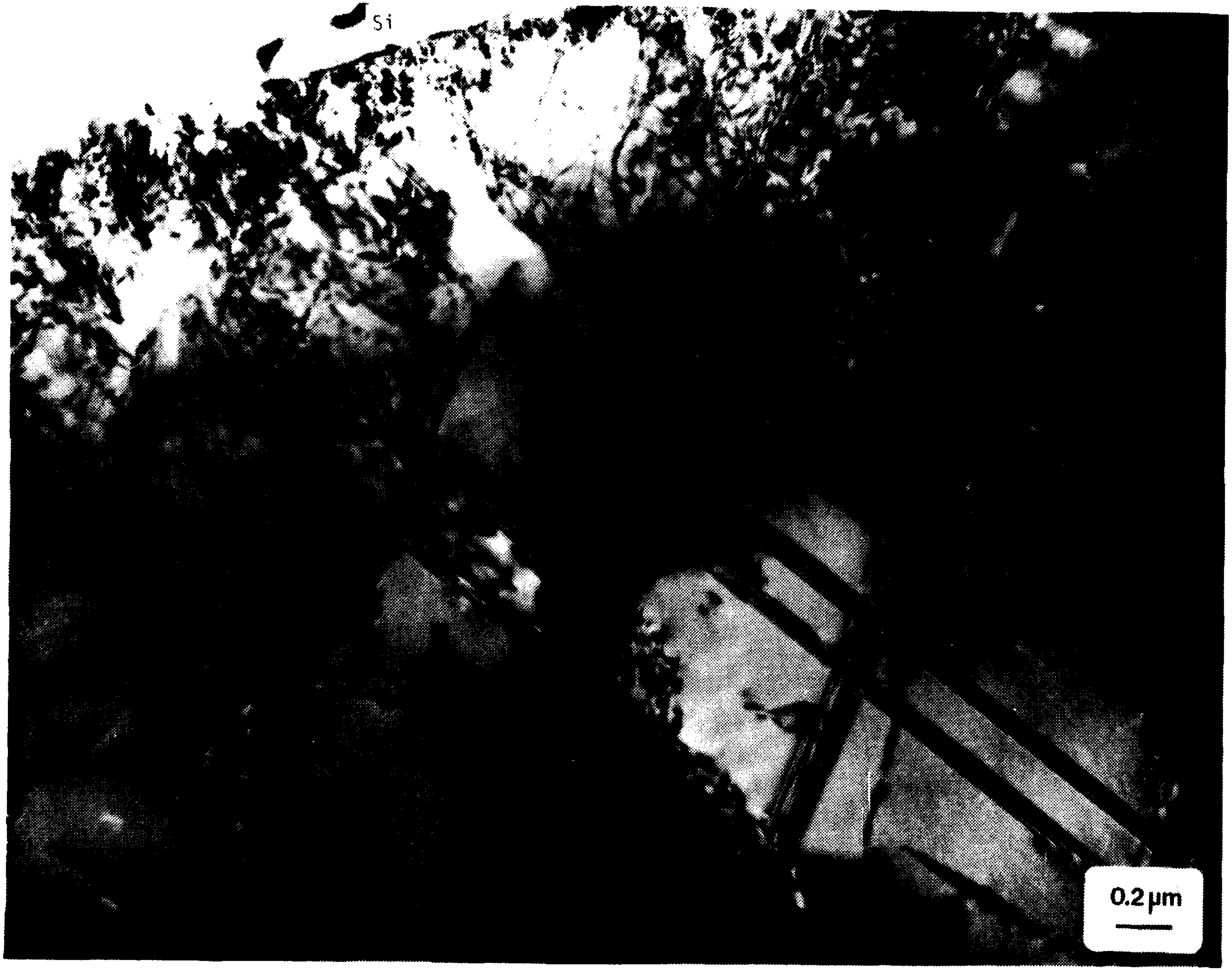

Figure 9. Cross-sectional TEM micrographs of single crystal thin film of undoped CVD β-SiC deposited on single crystal (100) Si at 1360°C and 4 atm. using a gas mixture of SiH_4, C_2H_4 and H_2. Micrographs shows full range of defects present in the as-grown film including stacking faults, partial and misfit dislocations and interfacial strain contrast. $\vec{g} = [022]$

Figure 10. Same as Figure 8 ($\vec{g}$ - [111]), except much higher magnification used to closely observe the strain contrast at the Si/SiC interface.

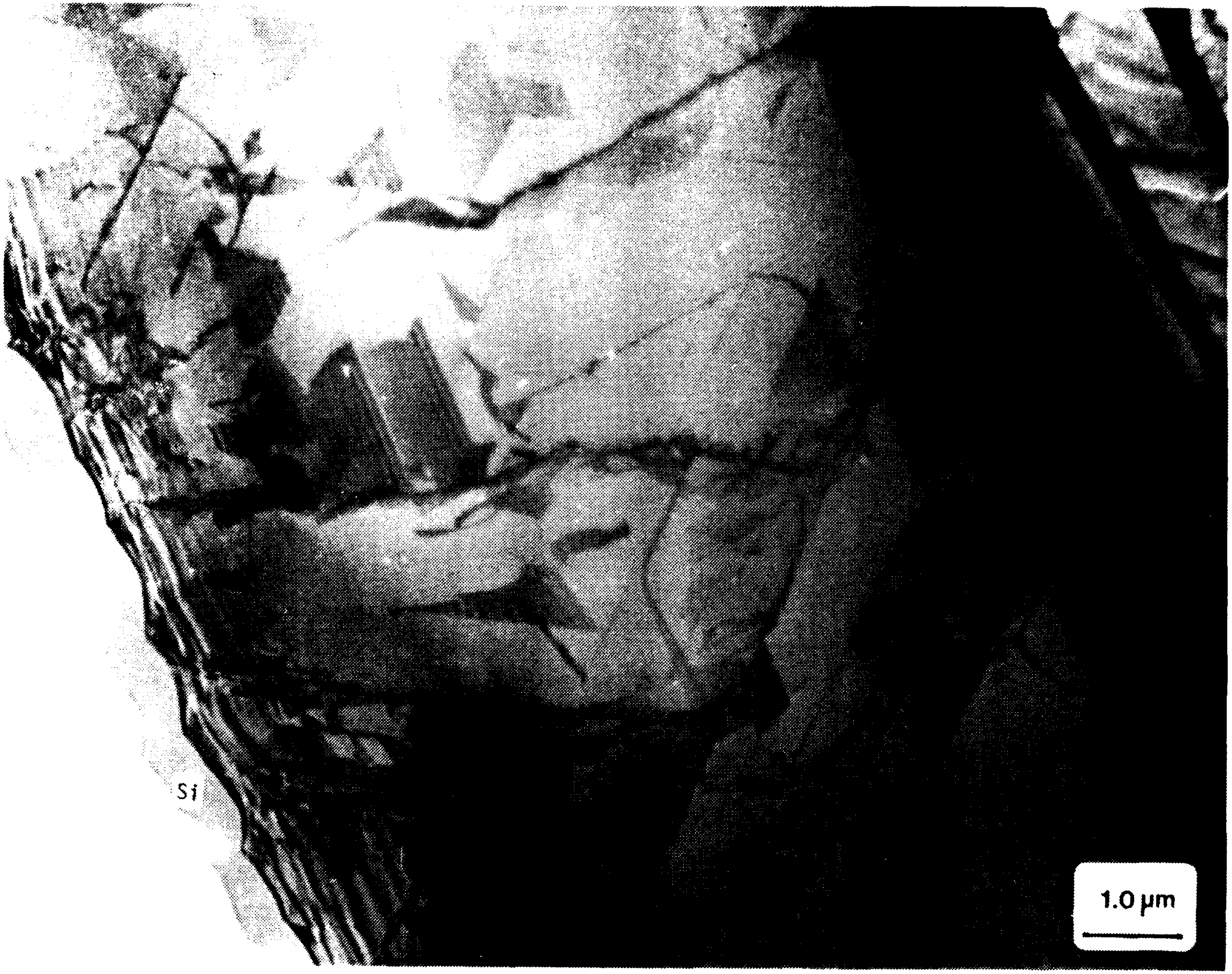

Figure 11. Cross-sectional TEM of β-SiC sample grown under the same conditions as noted in the caption of Fig. 8, except doped during growth with P (50 ppm in H_2) at a 2.4 x 10^{-8} atm. partial pressure (P concentration c̄s 5 x 10^{-6}) showing the considerable reduction in strain contrast at the Si/SiC interface with the removal of essentially all of the Si. Electron beam parallel to [011].

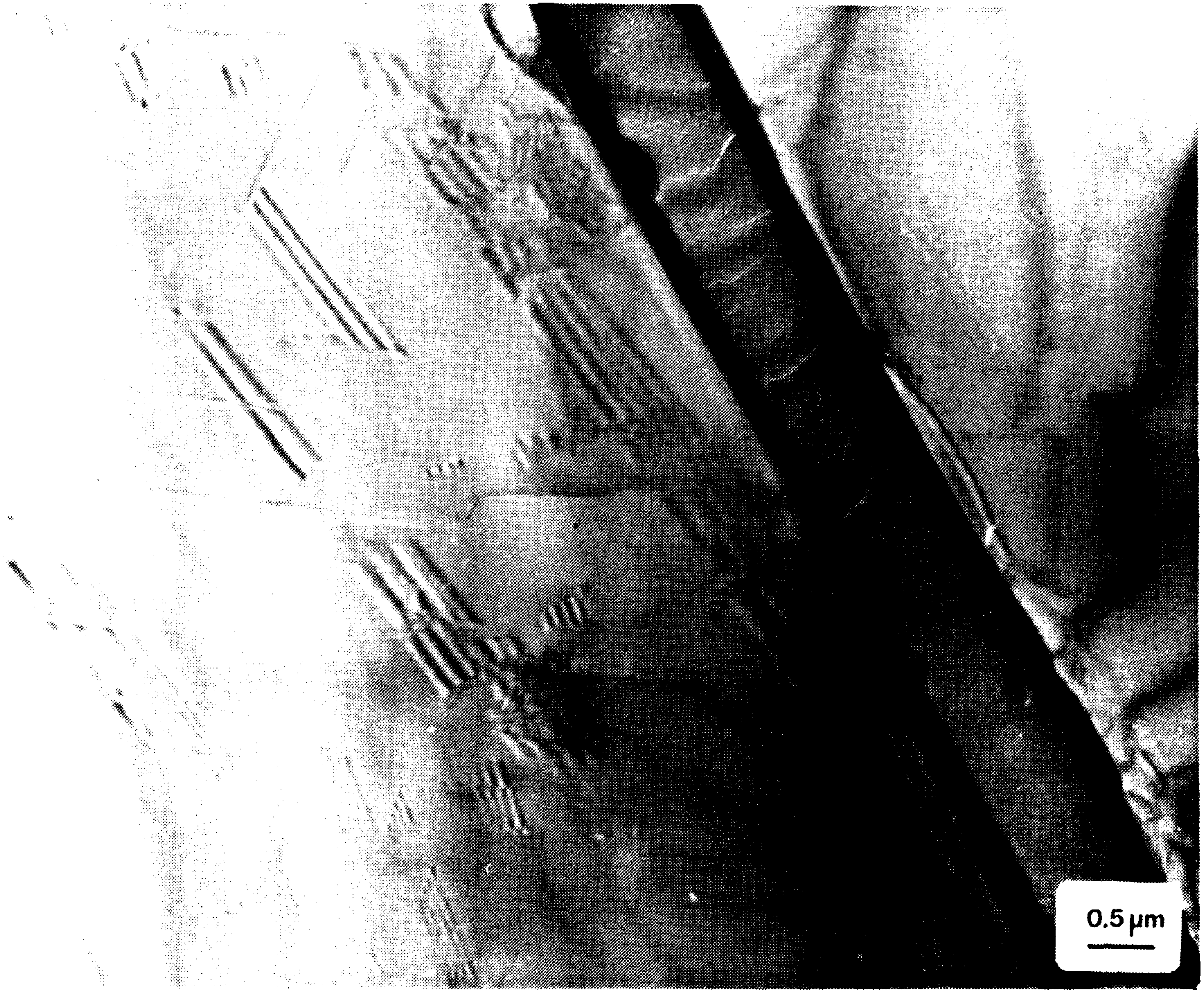

Figure 12. Same as Figure 11, except $\vec{g}$ = [200]. Also, in this figure one can observe stacking faults near the final growth surface.

As shown in Figs. 11 and 12 ($\bar{g}$ = [200]), the defect density decreases dramatically as moves toward the final growth surface (shown as black lines in these figures). Thus since devices are normally fabricated in the near surface regions, the substructure may not be particularly deleterious to device properties. Nevertheless the existence of elastic strain and the stacking faults and dislocations in all the thinner and thicker samples examined provides and impetus to conduct exploratory research using other substrates as described in the next section.

IV. OTHER CANDIDATE SUBSTRATE MATERIALS FOR THE GROWTH OF β-SiC.

In addition to the reasons noted above for exploring replacement substrates for Si, it must also be noted that we have ascertained that temperatures considerably above the melting point of Si are required to electrically activate the ion implanted impurities via thermal annealing. Thus in order to accomplish this each β-SiC film must be removed from the Si substrates and used alone or replaced with another substrate using techniques described in the next section. This step could possibly be eliminated if a more refractory substrate having a coefficient of thermal expansion and/or lattice constant close to that of β-SiC. Using these criteria, several candidate materials have been selected and procured. Table II indicates the cogent properties of each material. It is planned to conduct exploratory research using each of these materials during the next reporting period.

V. REMOVAL OF THE Si SUBSTRATE

As noted above and described in the following section, the annealing temperatures for electrical activation of implanted dopants via thermal heating has been found to considerably exceed the melting point of the Si substrate. As such a transfer process on as-grown thin 5μm films which removed the Si was attempted. The details of this method were given in the previous ONR report. Unfortunately as a result of the thinness of the films many of them cracked. As such, the use of these films has been abandoned in favor of thicker samples which are typically 12-17μm thick.

Table II. Cogent characteristics of particular materials which are candidates for substrates for the heteroepitaxial growth of Beta Silicon Carbide thin films.

Properties	SiC	Si	W	(Al_2O_3) Sapphire	Mullite	TiC	NbC
Structure	Cubic (Zinc-Blende)	Cubic (Zinc-Blende)	Cubic (BCC)	Rhombohedral	Orthorhombic	Cubic (NaCl)	Cubic (NaCl)
Lattice Parameter (A)	4.3590	5.4307	3.1652	a = 4.758 c = 12.991	a = 7.584 b = 7.693 c = 2.890	4.313	4.457
Thermal Expansion Coefficient	3.8 @ 200°C	2.5 @ 300°K	2.7 @ 300°K	8.4 @ 25-800°C	4.5 @ 25-1325°C	6.96 @ 298-2273°K	6.35 @ 298-2270°K
	4.3 @ 400°C	3.1 @ 400°K	4.4 @ 400°K	(60° to C-axis)	5.62 @ 25-1500°C	9.5 @ 298-2970°K	
	4.8 @ 600°C	3.5 @ 500°K	4.6 @ 500°K				
	5.2 @ 800°C	3.8 @ 600°K	4.7 @ 600°K				
	5.8 @ 1000°C	4.1 @ 700°K	4.7 @ 700°K				
	5.5 @ 1400-1800°C	4.3 @ 800°K	4.8 @ 800°K				
Melting Point (°C)	2830	1420	3387	2030	1850	3150	3760

Initial studies with the removal of the Si from the thick films using the process described in the last report also resulted in cracks in the films. In order to prevent this, a new method of removal has been developed which consists of (1) wax mounting the 12-17μm film face down on a beryllia substrate and (2) etching at room temperature in 1:1 HF:HNO_3 to remove the Si. The wax and sample holder must be insoluble in the acid mixture. Once the Si is removed, the wax is dissolved in trichloroethylene. Using this procedure the β-SiC film remains intact.

The resulting thicker films can be used alone if handled with care or may be reinforced by r-f sputtering another material on the surface of initial growth. Tungsten was previously selected as a candidate material because of its refractoriness, very low vapor pressure and the close match in thermal expansion with β-SiC. This material is also reported as being a good ohmic contact for n-type SiC. This result will be investigated during device fabrication.

Detailed descriptions of the sample preparation, implantation and annealing procedures, the last of which requires the removal of the Si substrate,are provided in the following sections.

VI. PREPARATION OF β-SiC FILMS FOR IMPLANTATION, OXIDATION AND DEVICE FABRICATION

The final surface of as-grown β-SiC is not sufficiently flat (variation of 0.1-0.2μm) for the fabrication of devices. It is also possible that this uneven surface decreases the measured mobility and increases the leakage current of the film. As such a polishing procedure has been developed to eliminate the wave-like nature of this surface. In this procedure each sample with its Si substrate is wax mounted Si side down on a 2.5μm precision machined and polished block have a variation in surface flatness within 0.00025μm across its diameter. The block and sample are then placed in a Syntron polishing/lapping machine containing an oiled nylon cloth work surface. One-tenth micron diamond paste serves as the polishing media.

Typically samples are polished for 48 hours. In that time, approximately 1500Å (the amount of as-grown surface roughness) of material is removed. Dektak profilometry results illustrated in

Fig. 13, indicates that the surface roughness disappears after the polishing procedure. However any differences in the total thickness of the film from one side to the other remains.

Cross-sectional TEM analyses have also been conducted on polished and polished/oxidized/etched samples to determine the extent of surface damage that results from polishing. Figure 14a shows the surface of a polished sample at a magnification of 200KX ($\vec{g}$ = [111]). As indicated by this figure, approximately 200Å of surface disorder results during polishing. This damage appeared under many diffracting contrast conditions. No particular type of defect is dominent. To remove polish-induced surface damage, as well as any surface contaminants introduced during growth, oxidation is performed using procedures described below. The standard oxidation presently used involves the growth of $\sim$5000Å of SiO_2 which removes nearly 1700Å of SiC. An STEM micrograph of a polished/oxidized/HF etched SiC sample is shown in Fig. 14b. Again, the magnification was 200KX and diffracting condition $\vec{g}$ = (111). As shown, virtually no surface damage remained after oxidation. In addition, the carrier concentration of $7 \times 10^{16}/cm^3$ was found to be very constant as a function of depth (up to 0.25μm) into the film (see section X for amore complete explanation of this aspect).

VII. ION IMPLANTATION AND ANNEALING

A. Overview

In this 6-month reporting period Al, P and B were implanted into β-SiC thin films, annealed at increasingly higher temperatures and measured for the onset of electrical activation of the implanted species and the amount of charg carrier present as a function of temperature. The results of each of these dopants will be discussed in turn in the following paragraphs.

Prior to implantation, each sample was polished, cleaned using the standard RCA routine and the surface damage removed via oxidation. This provides a clean and flat surface. In addition, sheet resistance, R_s, and the intrinsic effective carrier concentration, N_{eff}, were measured in order to have baseline data with which to compare the annealed samples.

POLISHING RESULTS - PROFILOMETRY

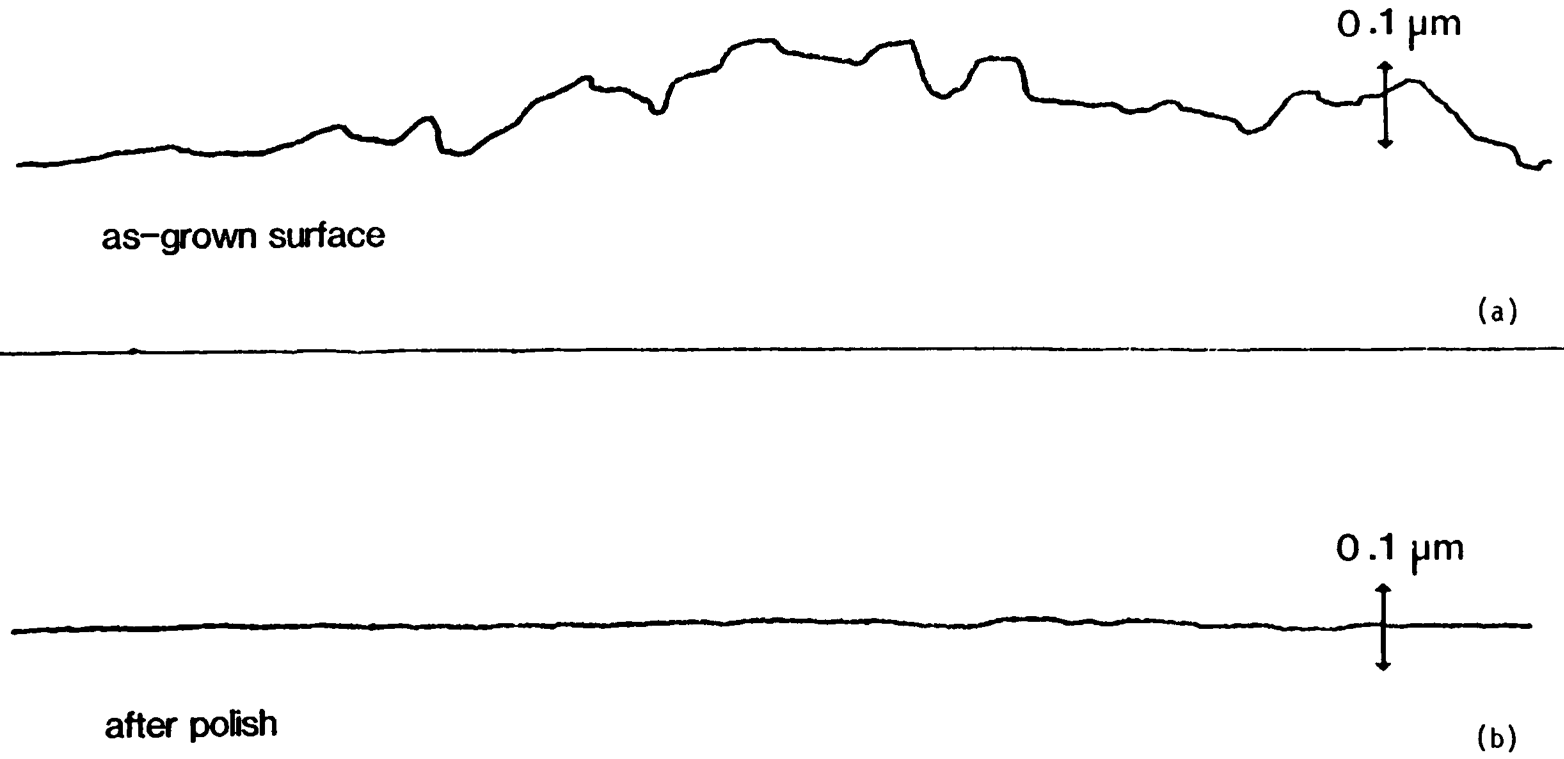

Figure 13. Dektak surface profile of SiC thin film deposited on Si (a) before polishing--sample has surface roughness of 0.1-0.2µm, (b) after polishing using 0.1µm diamond paste--surface roughness negligible.

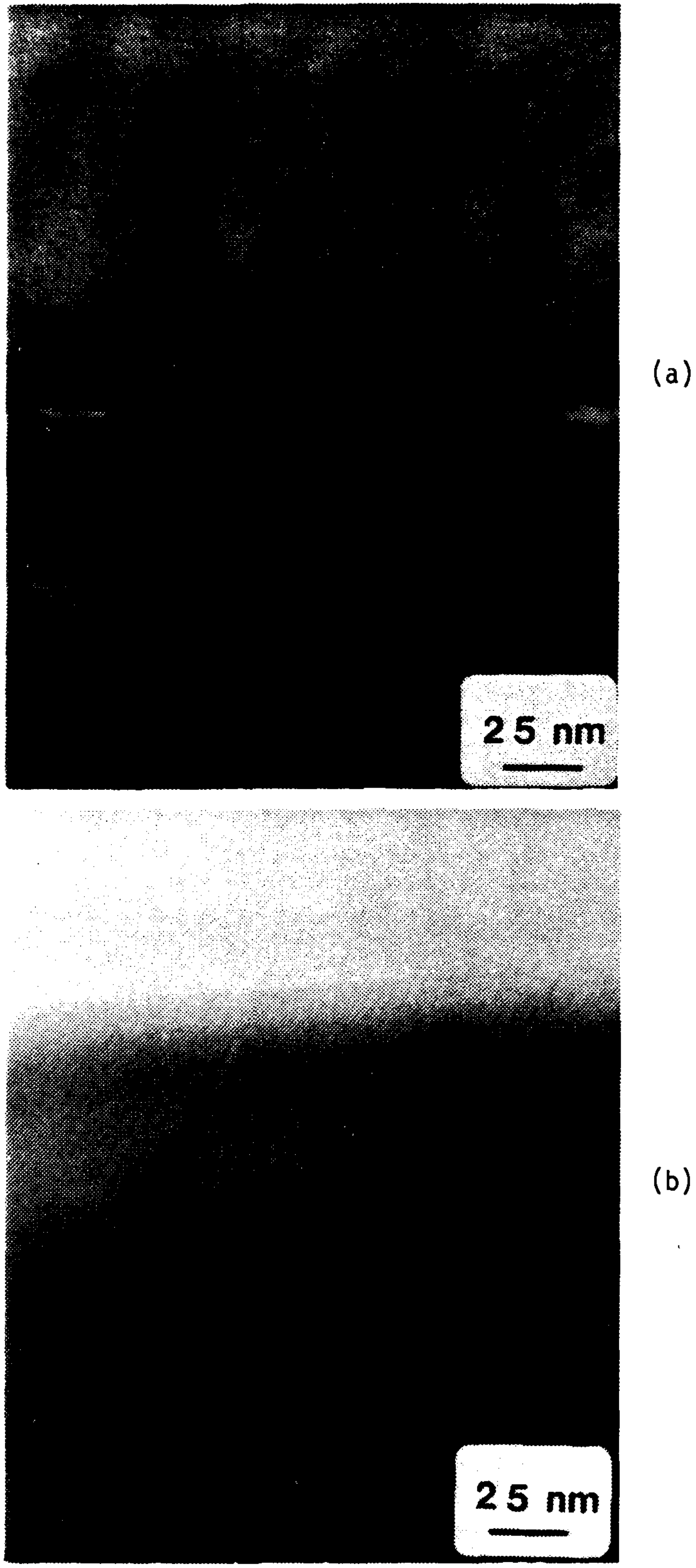

Figure 14. Cross-sectional TEM micrographs of the region at and near the top surface of β-SiC thin films showing (a) subsurface damage after polishing with 0.1μm diamond paste and (b) similarly polished sample after oxidation and resultant removal of this damage.

B. Aluminum and Phosphorus Implants

Prior to each implantation, each sample was polished, RCA cleaned and etched by oxidation (see Section VIII). This total scenario provides a clean flat surface for subsequent device fabrication. In addition, sheet resistance, R_s, and the intrinsic effective carrier concentration, N_{eff}, serve as initial electrical reference characterization of the as-grown samples.

Recently a low dose phosphorous (P) implant was completed using the following conditions. From LSS

Dose	$7.7 \times 10^{13}/cm^2$
NRG	110 keV
degree of offset	7°
temp of implant	ambient

theory, the projected range, R_p, of P in SiC at the above conditions is $R_p = 0.0921\mu m$. The fluctuation or straggle in R_p is $\Delta R_p = 0.0303$.

Figure 15 shows the profile of the concentration vs the depth determined with the ion microprobe for P-implanted SiC as well as the theoretical implant curve from LSS calculations using the same conditions noted above. These calculations assume the implant is made into an amorphous SiC. The projected range, R_p, of P in SiC for the above conditions is $R_p = 0.0921\mu m$; the fluctuation or straggle in R_p (denoted by ΔR_p) is 0.0303. The experimental peak concentration appears at 0.094μm which deviates only 1.9% from the LSS theoretical value of 0.9021μm. As noted in the previous ONR semi-annual report, the higher the atomic weight of the implanted species the better the agreement of theory with the experimental implant profiles.

To observe the structural surface damage caused by ion implantation, XTEM was again utilized. As shown in Fig. 16a (mag. = 100KX g = [111]), a 1600Å surface layer best characterized as point defect rich is evident. The first 200-300Å appears to be fairly defect free as the higher NRG electronic scattering events dominate the incident ion displacement. The center of the adjacent darker band is approximately 900Å from the sample surface. This coincides very well with the R_p value of 904Å obtained from SIMS

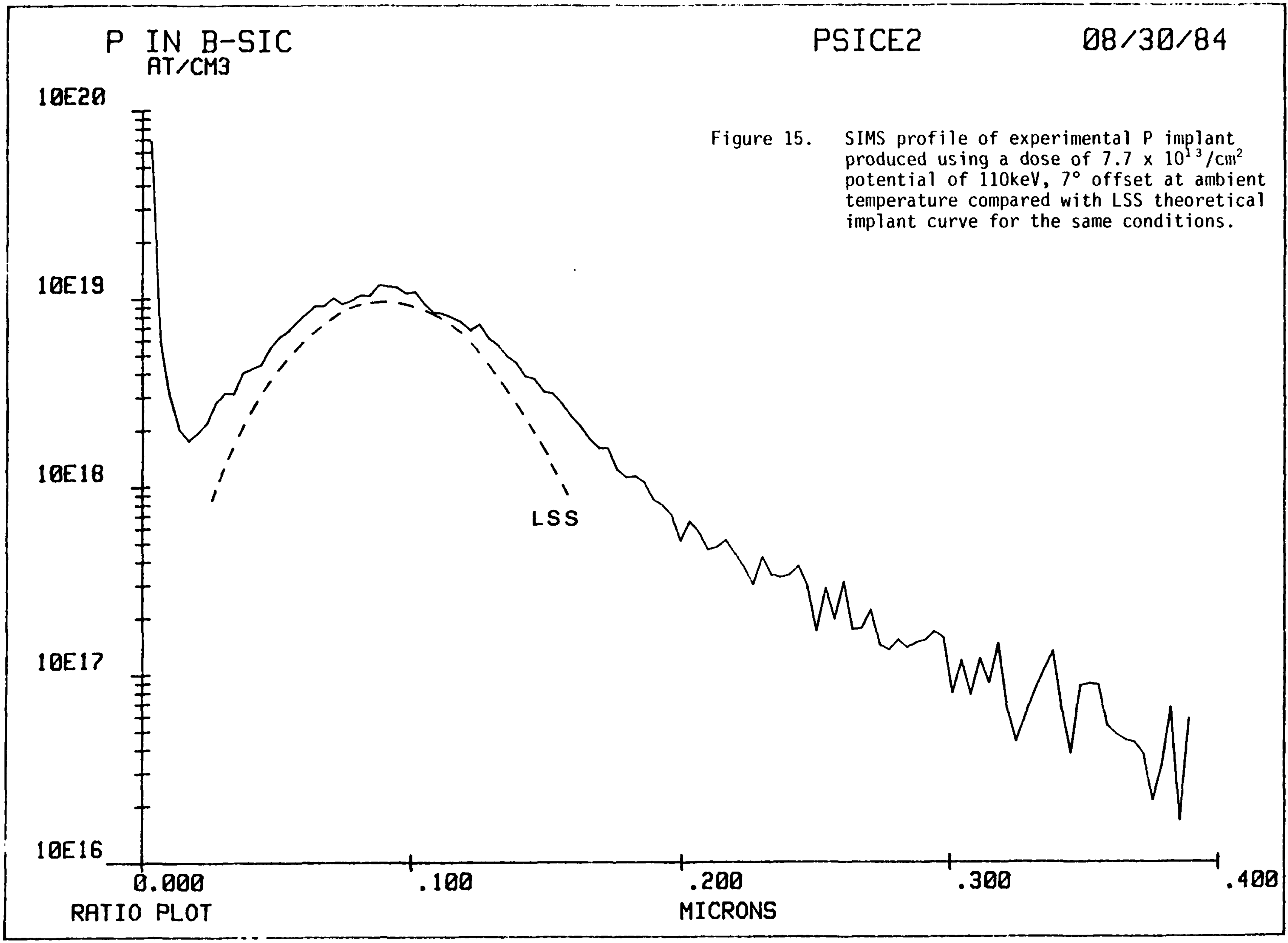

Figure 15. SIMS profile of experimental P implant produced using a dose of 7.7 x $10^{13}/cm^2$ potential of 110keV, 7° offset at ambient temperature compared with LSS theoretical implant curve for the same conditions.

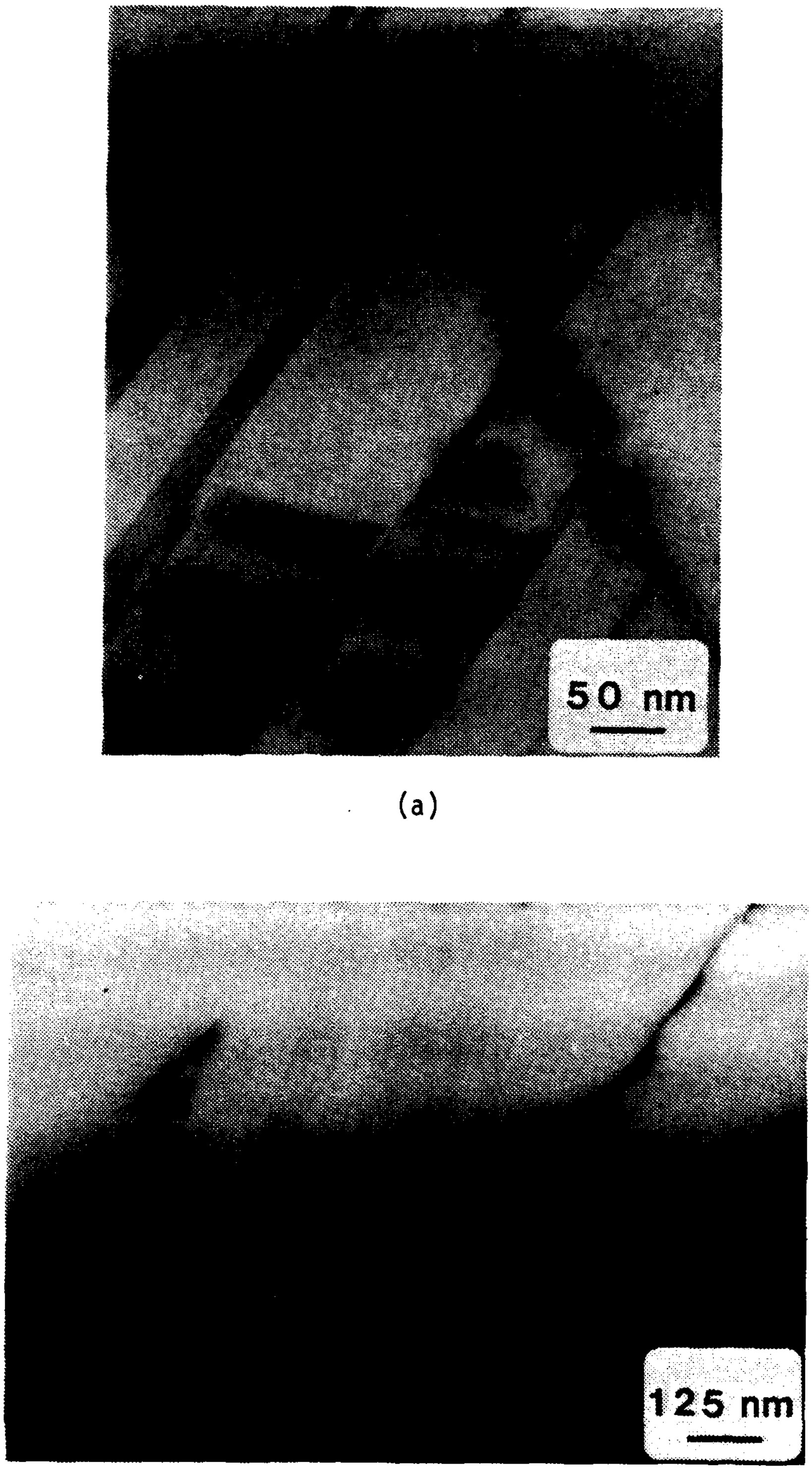

(a)

(b)

Figure 16. Cross-sectional TEM micrographs of a P implanted (dose = $7.7 \times 10^{13}/cm^2$, potential = 110 keV) β-SiC single crystal thin film showing (a) the as-implanted region (top one third of micrograph) with intersecting stacking faults and (b) same region after annealing at 1800°C for 3.5 min.

analyses. No amorphization occurred as indicated by the extension of stacking faults from the unimplanted region through the implanted region to the surface.

The determination of the proper annealing procedures for P implanted in β-SiC (as indicated above) is nearly complete. Table III is a summary of the results.

Table III. Summary of annealling results for P implanted into β-SiC. Implant conditions: dose = 7.71×10^{13}, NRG = 110 keV.

Anneal Temp (°C)	Anneal Time (min)	Ts (Ω/)	N_{eff} (cm^3)	Anneal Atmosph.
Preimplant	NA	40	4×10^{17}	NA
RT	NA	40	9×10^{17}(?)	NA
1000	10	40	NR	Argon
1100	10	40		
1200	10	40		
1300	10	40		
1400	10	39		
1440	5	38		
1500	5	37		
1550	5	37		
1600	5	34		
1700	3.5	25		
1740	3.5	23		
1800	3.5	18	$\sim 10^{18}$	
1900	2.5	18	NR	

The annealing system utilizes a highly purified SiC coated graphite heat strip sample holder. The heating rate is ∿34°C/sec. Samples were heated in argon at a pressure slightly less than one atmosphere. This aids in preventing SiC decomposition.

As shown in Table III, the intrinsic electron carrier concentration of the preimplanted sample was $4 \times 10^{17}/cm^3$. The C-V profile is given in Fig. 16. At a reverse bias value of 3.2 V, the leakage current increased quickly to 200μA. No further voltage was applied.

Following implantation a C-V measurement was done (i.e., RT anneal). As indicated in Fig. 17, the leakage current was very high at -.2 V. For that reason the N_{eff} value for the RT anneal is not credible. As indicated in Table III, R_s began to decrease past 1300°C annealing. After each anneal, C-V measurements were attempted.

However, no response was recorded until the 1800°C-3.5-minute anneal temperature was reached. The result is also shown in Fig. 16. Quite clearly the profile shape closely mimicks the SIMS profile with the peak being near the 0.09μm value previously determined. The effective carrier concentration value at this peak is, however, one order of magnitude lower than the implanted concentration of phosphorous atoms. The only conclusion to derive from this result is that at room temperature the activation combined with ionization of P is ∿10% of the maximum 10^{19} value. High temperature Hall effect measurements need to be conducted to determine N_{eff} with increasing temperature.

During the 1900°C-2.5-minute anneal the sample began to decompose. As indicated, R_s did not change from the value at 1800°C and N_{eff} could not be measured. A plot of annealing temperature vs R_s is shown in Fig. 18.

To observe the extent of P impurity diffusion of the 1800°C annealed sample, ion microprobe analysis was conducted. Figure 19 compares the concentration vs depth profiles of the as-implanted (preannealed) and annealed samples. As expected, the annealed profile peak became marginally depressed and widened. It deems fair to conclude that, as far as devices are concerned, diffusion of P during annealing is insignificant.

Cross-sectional TEM was also utilized to observe the extent of damage recovery in the low dose P implant sample shown in Fig. 16a. As shown in Fig. 16b, the defect-rich surface appears to have structurally recovered to a large degree after the 1800°C anneal. However, the intrinsic defect density of the sample as a whole does not appear to have decreased.

In addition to the P implant, a dual Al implant has been completed using the following implant conditions:

Dose (1) = 9 x 10^{14}/cm^2 Dose (2) = 6 x 10^{14}/cm^2
Energy (1) = 190 keV   Energy (2) = 110 keV
degree of offset = 7°
temperature = ambient

Figure 20 shows the ion microprobe concentration vs depth profile for the two implants. The two LSS profiles are plotted as a

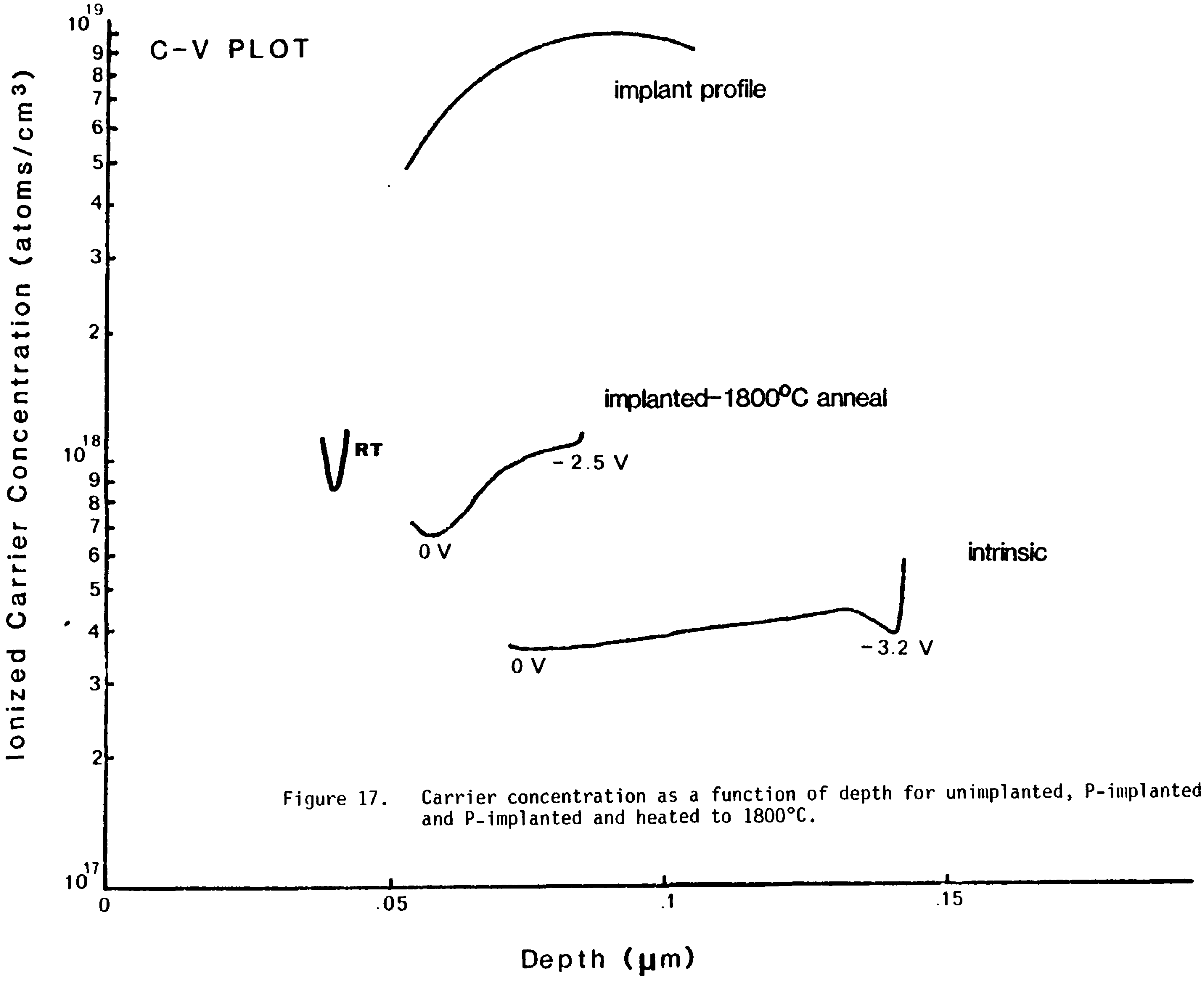

Figure 17. Carrier concentration as a function of depth for unimplanted, P-implanted and P-implanted and heated to 1800°C.

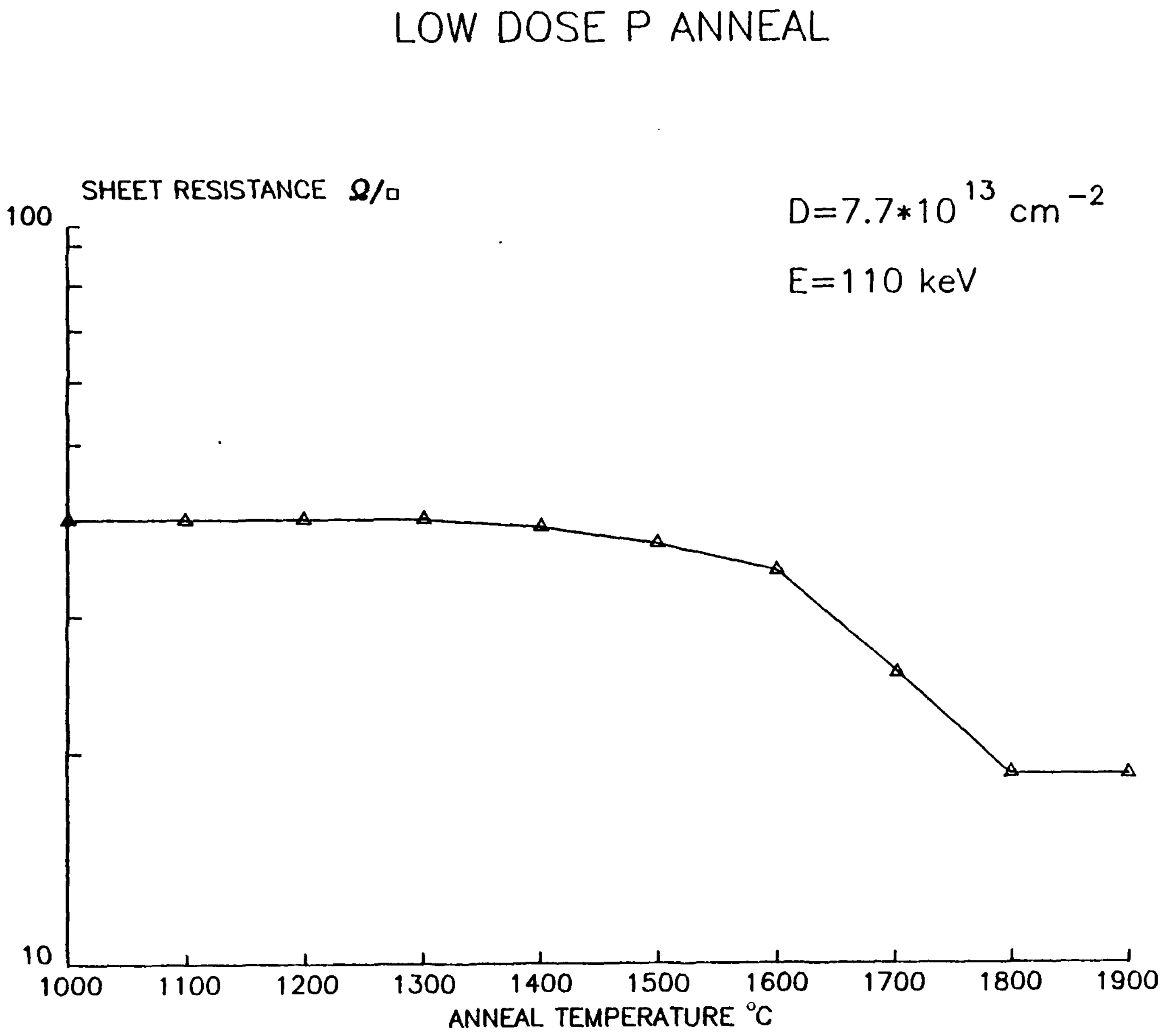

Figure 18. Sheet resistance as a function of annealing temperature for a P-implanted β-SiC (dose = 7.7 x 10^{13} cm^2 at 110 keV) thin film.

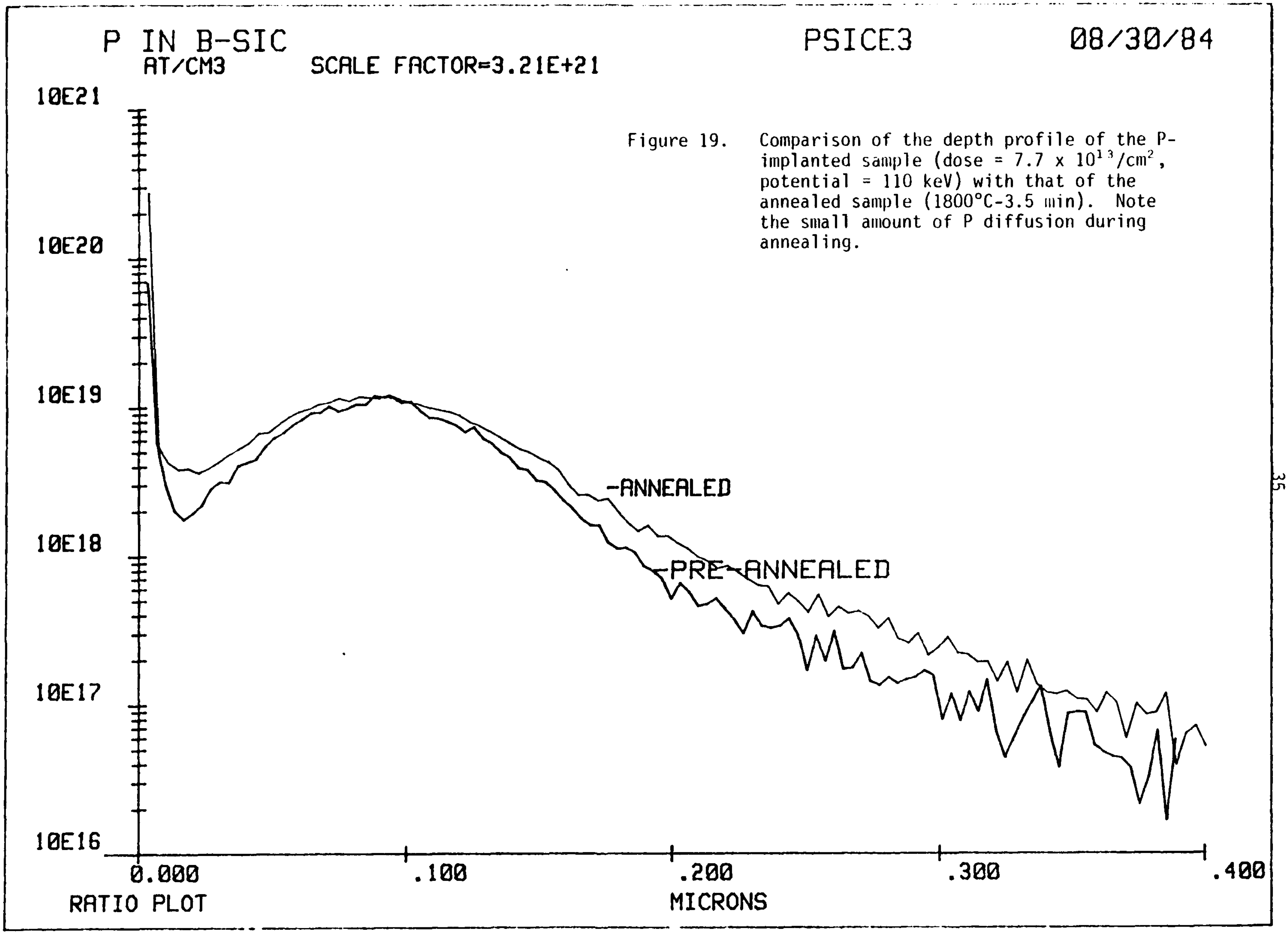

Figure 19. Comparison of the depth profile of the P-implanted sample (dose = 7.7 x $10^{13}/cm^2$, potential = 110 keV) with that of the annealed sample (1800°C-3.5 min). Note the small amount of P diffusion during annealing.

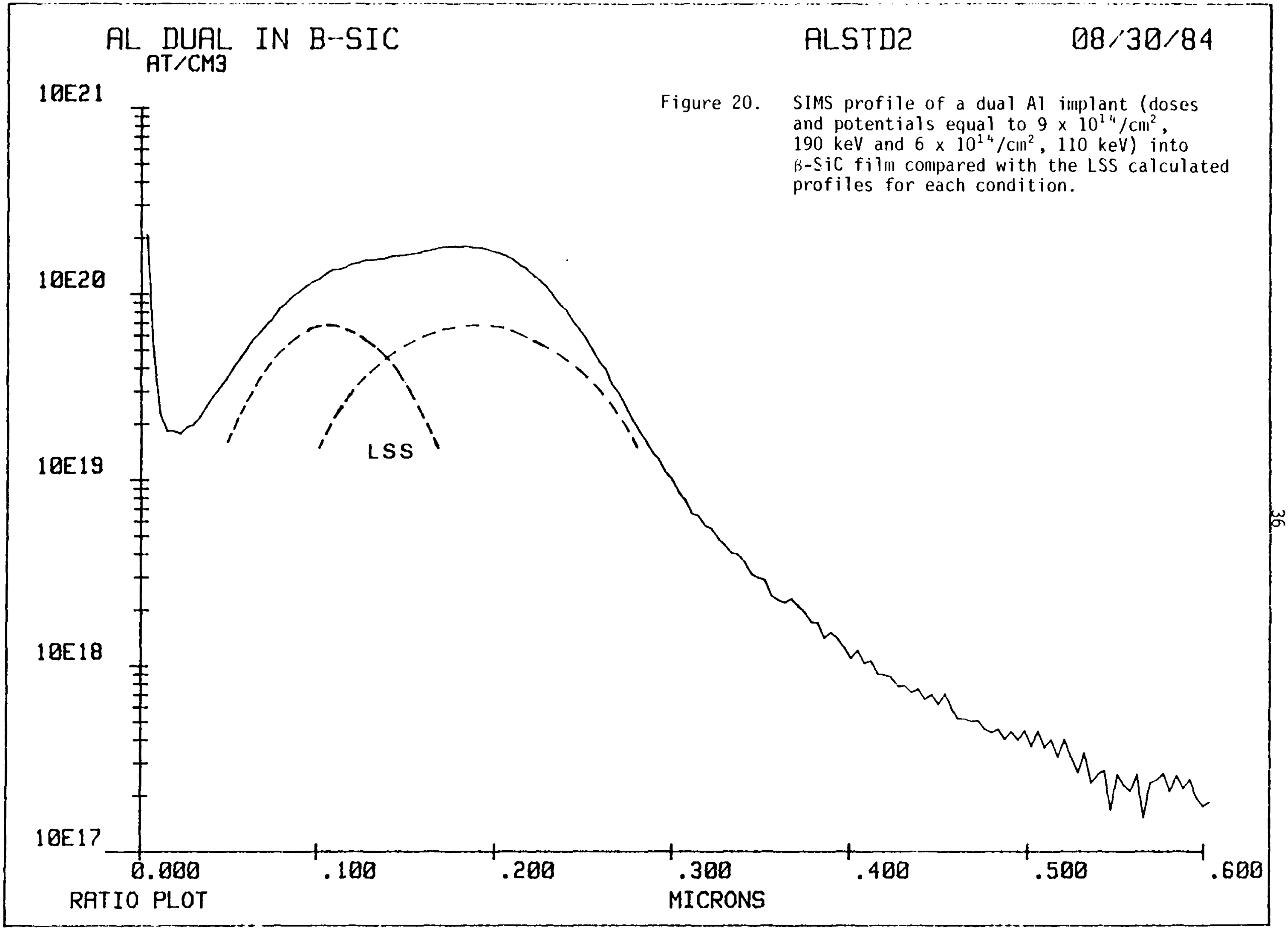

Figure 20. SIMS profile of a dual Al implant (doses and potentials equal to 9 x $10^{14}/cm^2$, 190 keV and 6 x $10^{14}/cm^2$, 110 keV) into β-SiC film compared with the LSS calculated profiles for each condition.

comparison. Quite clearly the two implants are additive resulting in a nearly flat peak at a concentration value twice the value of either implant. It is evident that with the use of this multiple implant, a flat profile and sharp junction can be obtained.

Figure 21 is a XTEM micrograph of the Al implanted surface at a magnification of 100KX. As shown, an amorphous layer resulted. Closer observation shows that the immediate surface is fairly defect-free. Again, this is caused by the domination of the electronic scattering rather than nuclear scattering. The most clear amorphous region appears near 0.15μm corresponding to the median in the SIMS profile. As one continues further away from the implant center, microcrystallinity appears to increase to the amorphous/crystalline interface. The overall degree of amorphization appears to be low.

The annealing research for this type of implant is currently ongoing. In addition, characterization of a P triple implant and an Al quadruple implant will be conducted.

C. Boron Implants

Boron has been double implanted into thick ($\sim$15 m) β-SiC films using the following conditions:

Dose (1) 1 x $10^{15}/cm^2$ Dose (2) 7.6 x $10^{14}/cm^2$
Energy (1) 200 keV Energy (2) 100 keV
degree of offset = 7°
temperature = ambient

This gives a peak concentration of 5 x $10^{19}/cm^3$. Annealing studies similar to those used for the P research noted above.

VIII. OXIDATION STUDIES

Oxidation has been achieved using a flowing wet O_2 atmosphere at both 1100° and 1200°C. Although it was obvious that an oxide film was present, because of color changes and perfect electrical insulation, thickness measurements presented a prolonged problem. It was originally thought that oxide thickness could be determined using a Nanometrics "Nanospec," which is a reflectance device used in the silicon industry. Upon discussion with the manufacturers, it was decided that with some adjustment, the "Nanospec" could be "fooled" into thinking that the SiC film upon which the oxide was grown was

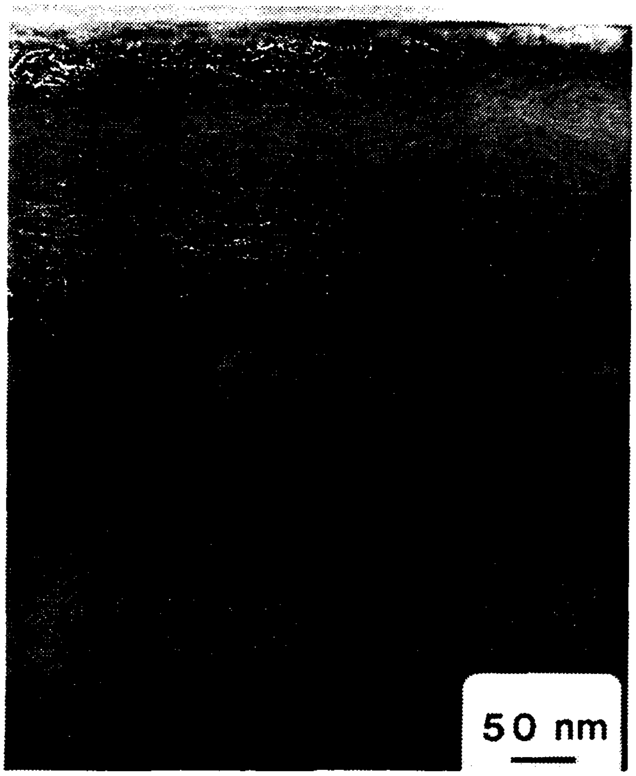

Figure 21. Cross-sectional TEM of P double implant (doses and potentials equal to 9 x $10^{14}/cm^2$, 190 keV and 6 x $10^{14}/cm^2$, 110 keV) into β-SiC film (see top one-half of figure). The implanted region is amorphous with a maximum concentration at approximated 0.15μm from the surface.

Figure 22. Angle lapped sample of SiO_2/β-SiC/Si at a 36' angle to produce a magnification of 100X. The magnification of the photographic 400X. The dark bands are color fringes in the oxide. The actual oxide/SiC interface is not visible because the SiC does not provide sufficient reflectance to show this interface.

actually Si, and thus be able to obtain an accurate measurement of oxide thickness. However, the SiC was found to be too transparent to provide sufficient reflectance at the SiC/oxide interface.

The next method employed to determine the oxide thickness was angle lapping of the oxide/film/Si substrate combination. The oxidized samples were lapped at a 36 minute angle (100X) with 0.25μm diamond paste, and subsequently polished in Syton. They were examined under a microscope using a Nomarsky lens, photographed, and the layers measured with a ruler. However, it was extremely difficult to determine the positions of the SiC/oxide interface as well as the top surface of the oxide. The best picture obtained can be seen in Fig. 22. The inability to find the interface is due, in part, to the degree of surface roughness caused by the oxidation, which can be observed in this picture. This roughness can be as much as 1500Å. More important, however, is the fact that the SiC does not provide enough reflectance to show the interface. The two dark bands are just color fringes in the oxide. The actual interface is somewhere between the point where the regular, smooth fringes in the SiC stop, and the first observed color fringe.

The third method attempted was to use a profilometer to measure a step in the oxide. In this method, the oxide layer is partially masked with wax and the exposed oxide is etched away with buffered oxide etchant. The was is then removed, leaving an oxide layer with a step down to the SiC. A Dektak profilometer, utilizing a sensitive stylus, is then used to measure the oxide step. This method gave the best results, yet measurements were still quite inaccurate because of the surface roughness of the SiC, which was also replicated by the oxide. The measurements were still only accurate to within ±500Å (see Fig. 13 for profile of unpolished surface).

Because of this measuring inaccuracy, and other concerns, it was decided that the as-grown samples must be polished. Polishing was performed on a Syntron polishing system using 0.1μm diamond paste on a nylon knap. The observed roughness on polished SiC is negligible. Step measurements of the oxide layers grown in this polished SiC were considerably easier and resulted in interpretable and repeatable data as shown in Fig. 23. The SiC part of the profile

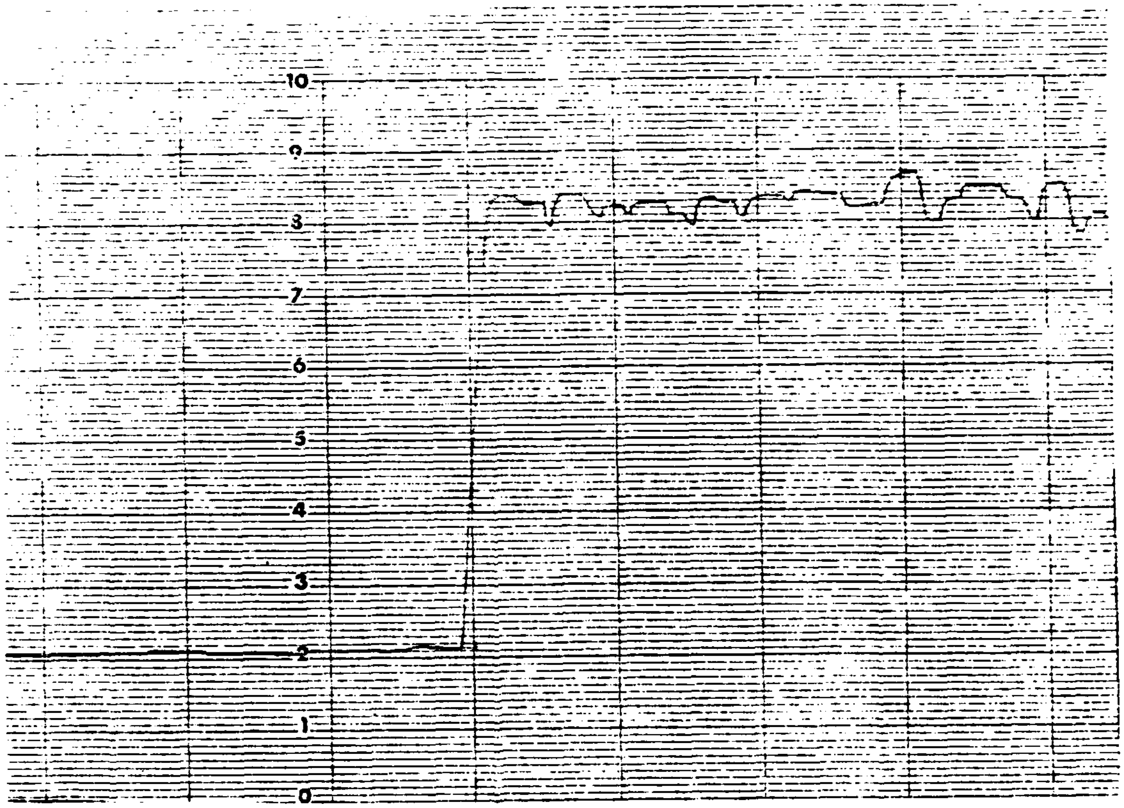

Figure 23. Profilometer determination of the oxide thickness thermally grown on a polished β-SiC thin film at 1200°C in flowing (60 ccm) wet O_2 for 780 minutes. Polished SiC film surface roughness is shown in the left portion of the diagram while a similar profile is shown for the oxide film in the right portion of the graph. Each minor division is equal to 200Å.

is smooth, and the steps are abrupt. There is, however, some surface roughness on the oxide layer. The roughness increases with oxidation time and thickness. For a thickness of 2700Å, the observed surface roughness is around 250Å; however, at a thickness of 12,300Å, the observed roughness is up to 1400Å. This roughening could possibly be due to partial crystallization of the SiO_2 into crystobalite, but this has not been studied at this time.

Angle lapping was also performed on polished samples. While the roughness was not a problem, it was still impossible to determine the position of the interface. As such it was decided that the profilometer provides the most accurate results.

The results of wet oxidation studies on intrinsic SiC at 1000°, 1100° and 1200°C are shown in Fig. 24. This wet oxidation was achieved by bubbling O_2 through deionized water at 98°C, at a flow rate of 60 ccm. Varying flow rates have been used, from 3 ccm to 60 ccm. It was found that, while oxidation was considerably slower at 3 ccm, there was no rate change between 20 and 60 ccm. Therefore, it is assumed that a flowrate of over 20 ccm should give the maximum oxidation rate at a given temperature. These curves exhibit the expected linear-parabolic nature of oxidation of SiC, with oxidation being faster in the initial regime, and slower after the diffusion of oxygen through the oxide layer becomes the controlling factor.

The color of the oxide layer changes with thickness, because there is constructive interference of only one visible wave length for a certain oxide thickness. The colors and thicknesses observed for SiO_2 on SiC follow exactly those observed in SiO_2 on Si. One can actually tell, to within 100-200Å, how thick an oxide layer is by simply noting the color. For example, it has been determined that the oxidation rate of B-doped SiC is markedly slower than that of intrinsic because of the observed color differences. The effects of doping on oxidation rates will be studied in the future.

During thermal oxidation, some of the SiC is consumed. For device manufacture it is important to know how much SiC is consumed in realtion to how much oxide is grown. A theoretical calculation can be made using atomic densities:

$$X_{SiC} = \frac{N_{ox}}{N_{SiC}} X_{ox}$$

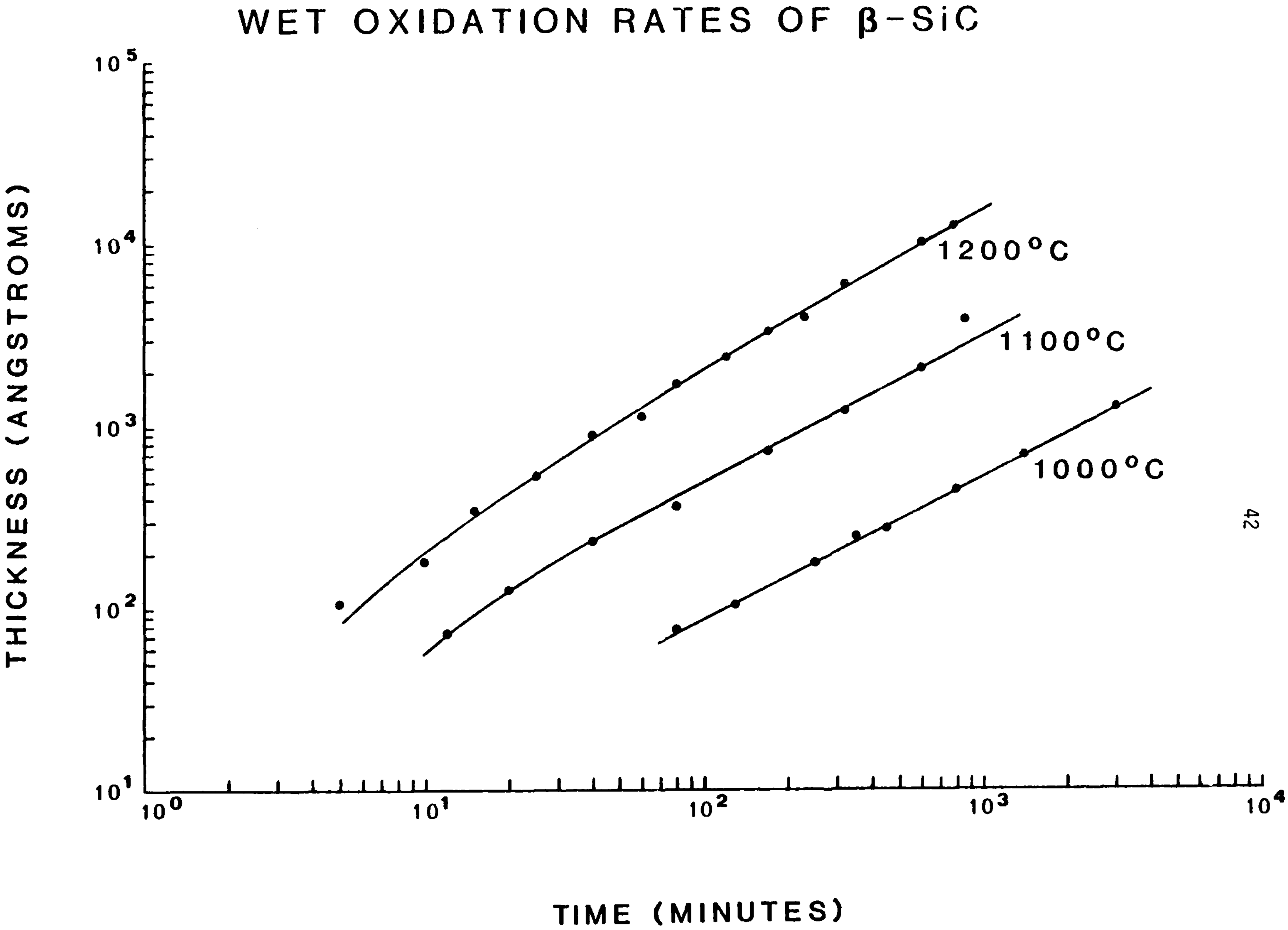

Figure 24. Thickness of oxide layer grown on an intrinsic β-SiC thin film by bubbling O_2 through deionized H_2O at 98°C at a flow rate of 60 ccm for the various times and temperatures shown on the graph.

where X_{SiC} = thickness of SiC consumed

X_{ox} = thickness of oxide grown

N_{SiC} = density of Si atoms in SiC (4.83×10^{22} Si atoms/cm^3)

N_{ox} = density of SiO_2 molecules in oxide (2.3×10^{22} molec/cm^3)

or $X_{SiC} = .476\ X_{ox}$

This value was checked experimentally by angle lapping a bare SiC layer, determining its thickness, then oxidizing and angle lapping again. From this experiment, the "consumption factor" was .34-.37. It is suggested that these experimental values are not accurate because of the technique used, and that values closer to theoretical will be obtained with more precise techniques.

IX. PLASMA ETCHING STUDIES

Because of the need to perform surface removal and mesa etching, a method of etching SiC is needed. Because there is no suitable wet etchant for SiC, dry etching processes have been investigated. Sputter etching with Ar at 100 watts was found to give an etch rate of 33Å/min. While this yields a faster rate of removal than oxidation, it is undesirable because sputter etching involves physical damage, such as the formation of dislocations and amorphous regions. In silicon, damage has been found as deep as 500-750Å, from the sample surface.[10] This damage has negative effects on interface state densities, minority carrier generation times, breakdown voltages, barrier heights, and trapping levels.

To avoid this damage, plasma etching has been investigated. In this process, the sample is located on the grounded electrode; thus, there is very little ion bombardment. The gas system used initially was $CF_4 + O_2$. The F etches Si via the formation of SiF_4, while the O_2 reacts with the C in SiC, and the C in DF_4, to form CO and CO_2. This gas system was investigated by Matsui[11] but employed for reactive ion-beam etching of SiC. This investigator found the optimum mixture to be at 40% O_2.

The samples were masked with photoresist, and etched using a Technics Planar Etch II at 2 torr and 200 watts RF power. The resulting etch rates for warying O_2 mixing ratios have been very inconsistent. While there is a general increase in etch rate as

% O_2 increases, it is impossible to derive a curve from the data. At the same mixing ration, time, power, pressure, etc., one can never get the same rate twice. Etch rates have been obtained in the range of 150Å/min to 550Å/min.

These etch rates are significantly higher (∿2½ times higher) than those reported by Matsui et al.[11] However, this could be caused by a difference in the power used. The cause for the non-reproducible results, at this time, is assumed to be poor flow control.

While the etch rates were desirably fast, all the samples contained a dark surface layer. The layer, approximately 1000Å thick after 20 minutes etching, was assumed, at first, to be C. However, the layer did not burn off at 1000°C in air, nor did it etch away in hot nitric acid. After SIMS analysis, it was determined that the layer was actually redeposited SiC. There was virtually no difference between the bar graphs for unetched SiC (Fig. 25) and the dark surface layer of etched SiC (Fig. 26). It is assumed that the layer is amorphous or polycrystalline and is loosely bound to the single crystal SiC surface, because it scratches away easily. The redeposited layer can also be removed by (1) oxidizing for a sufficient time to consume 1000Å of SiC and (2) etching away the oxide layer leaving a bare, etched SiC surface. This type of layer was not reported by Matsui et al.[11] However, it is assumed that this layer would not form in his process; since, reactive ion beam etching involves ion bombardment, which would sputter away any redeposited material. The thickness of the layer also increases as etch time increases, thus retarding the etch rate at longer times.

The "SiC" layer appears regardless of the power levels, although it is thinner at 50 watts than it is at 200 watts. However, the etch rate is also slower at 50 watts. It is possible that the redeposited layer could be avoided at lower pressures, because there would not be as many molecules to combine and redeposit. Etching at lower pressures has not been attempted at this point because it is very hard to control mixing ratios accurately below 2 torr with the flow meters on this system.

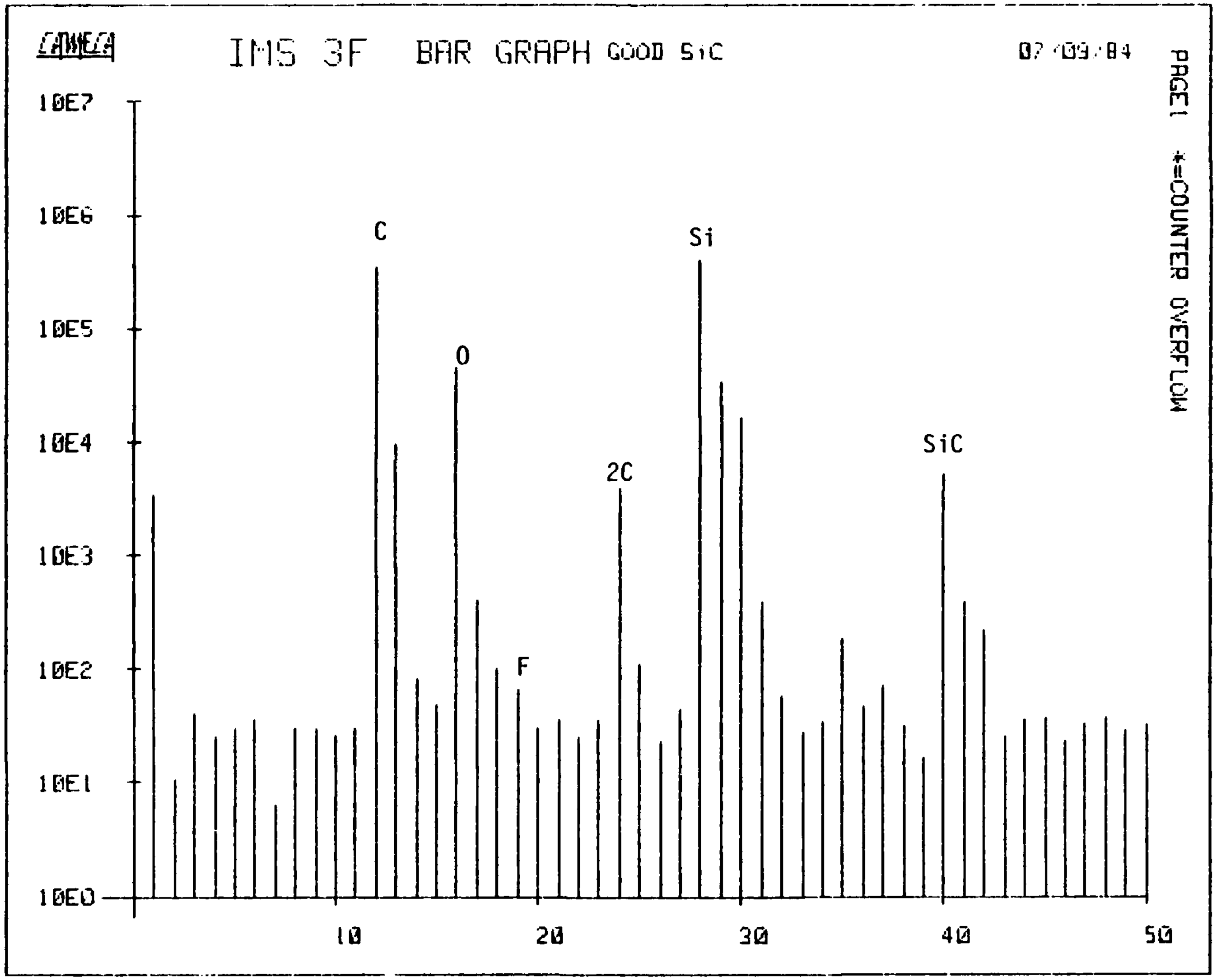

Figure 25. Bar graph resulting from SIMS chemical analysis (mass scan) showing count rate for the various elements or molecules having a mass/charge ratio shown on the abscissa for a nonplasma-etched intrinsic β-SiC single crystal thin film.

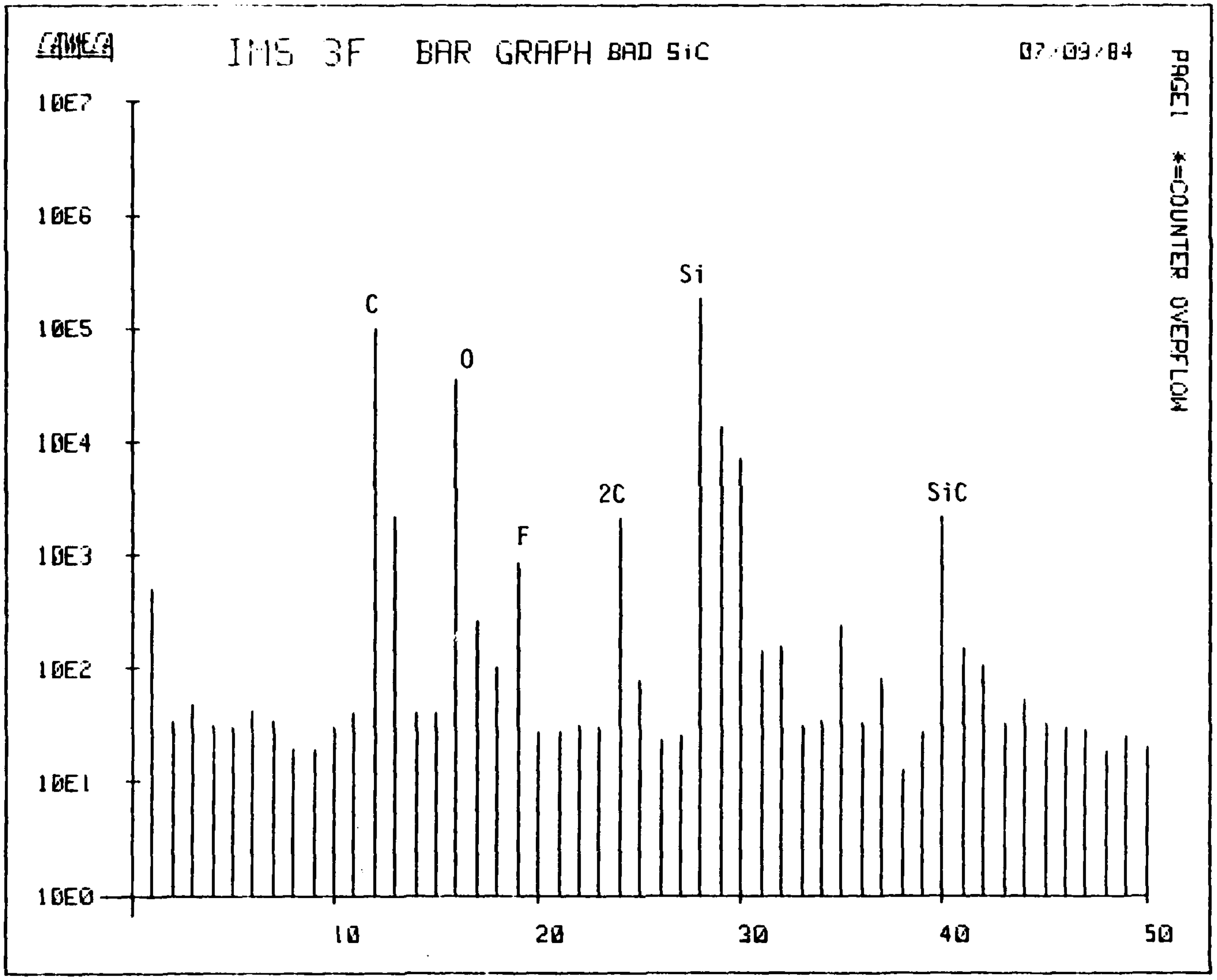

Figure 26. Bar graph resulting from SIMS chemical analysis (mass scan) showing count rate for the various elements or molecules having a mass/charge ratio shown on the abscissa for the surface layer produced by plasma etching of a β-SiC intrinsic single crystal thin film. Note similarity with Fig. 25.

X. ELECTRICAL CHARACTERIZATION

A. Equipment

In order to more fully and more accurately electrically characterize the as-grown β-SiC thin films as well as those which had been doped during growth or by ion implantation and the devices subsequently produced in the films, an electrical characterization laboratory has been established. The individual pieces of equipment which have been purchased and their use is as follows:

1. Miller Feedback Profiler
   - a) Measurement of active carrier concentration of planar wafers using an associated Hg probe and the differential C-V method.
   - b) Measurement of junction capacitance of devices using the probe station noted below.
2. Hewlett Packard 4145A Semiconductor Parameter Analyzer
   Measurement of I-V characteristics of thin films and devices and the analyses, transport factors and other transistor constants, used in conjunction with the probe station noted below.
3. Rucker and Kolls Probe Station
   - a) Used with the Miller Feedback Profiler for measurement of junction capacitance.
   - b) Used with HP 4145A for measurement of I-V characteristics of thin films and devices.
   - c) Measurement of various parameters for integrated circuits.
4. Signatone Four Point Probe and associated equipment
   Measurement of sheet resistance
5. Thermocompression bonder for lead wire attachment
6. High Temperature (up to 400°C) Hall effect measurement system

B. I-V Measurements and Schottky Diodes

As noted in Section VI, as-grown β-SiC thin film samples contained surface variations of approximately 0.1-0.2μm in height. Polishing with 0.1μm diamond paste and subsequent oxidation and etching with HF acid not only removed the subsurface damage induced by polishing but also gave a very uniform carrier concentration of $7 \times 10^{16}/cm^3$ into the film, as shown in Fig. 27. Figure 28 shows the I-V characteristics of a back-to-back Schottky diode produced on a thick (∿10μm) β-SiC film which had been removed from the Si substrate using a 50-50 mixture of HF and HNO_3 to dissolve the Si. The film had also been previously polished, oxidized and etched on the final grown surface before the In (ohmic) and Au (rectifying) contacts were produced. However the leakage current was not significantly decreased from that of the unpolished sample. Thus it may imply that the leakage current was caused by the presence of lattice defects and the generation current which is caused by their existence in the solid.

C. Hall Measurements

Hall measurements have also been conducted during this reporting period on as-grown and polished, oxidized and etched β-SiC thin films. The results of these measurements on two samples are given in Table IV below:

Table IV. Temperature dependence of Hall effect data for as-grown and polished, oxidized and etched β-SiC thin films.

Sample #	Description	Temp. (K)	Carrier Concen. (cm^3)	Resistivity (ohm - cm)	Mobility (cm^2/V-S)	Type
831215	as-grown	77	2.8×10^{16}	0.25	901	n
	thin sample (4 m)	296	6.4×10^{17}	0.133	73	n
		473	2.3×10^{18}	0.07	38	n
840509	polished, oxidized and etched	77	5.6×10^{16}	0.37	298	n
		296	8×10^{17}	0.054	144	n

From these results the ionization energy of the electrically-active donor-type species from 77°K to 296°K is just 0.028 ev which is smaller than the reported value of ionization of N in β-SiC (0.05 ev).[12] This suggests that the unknown donor character does not come from the presence of N.

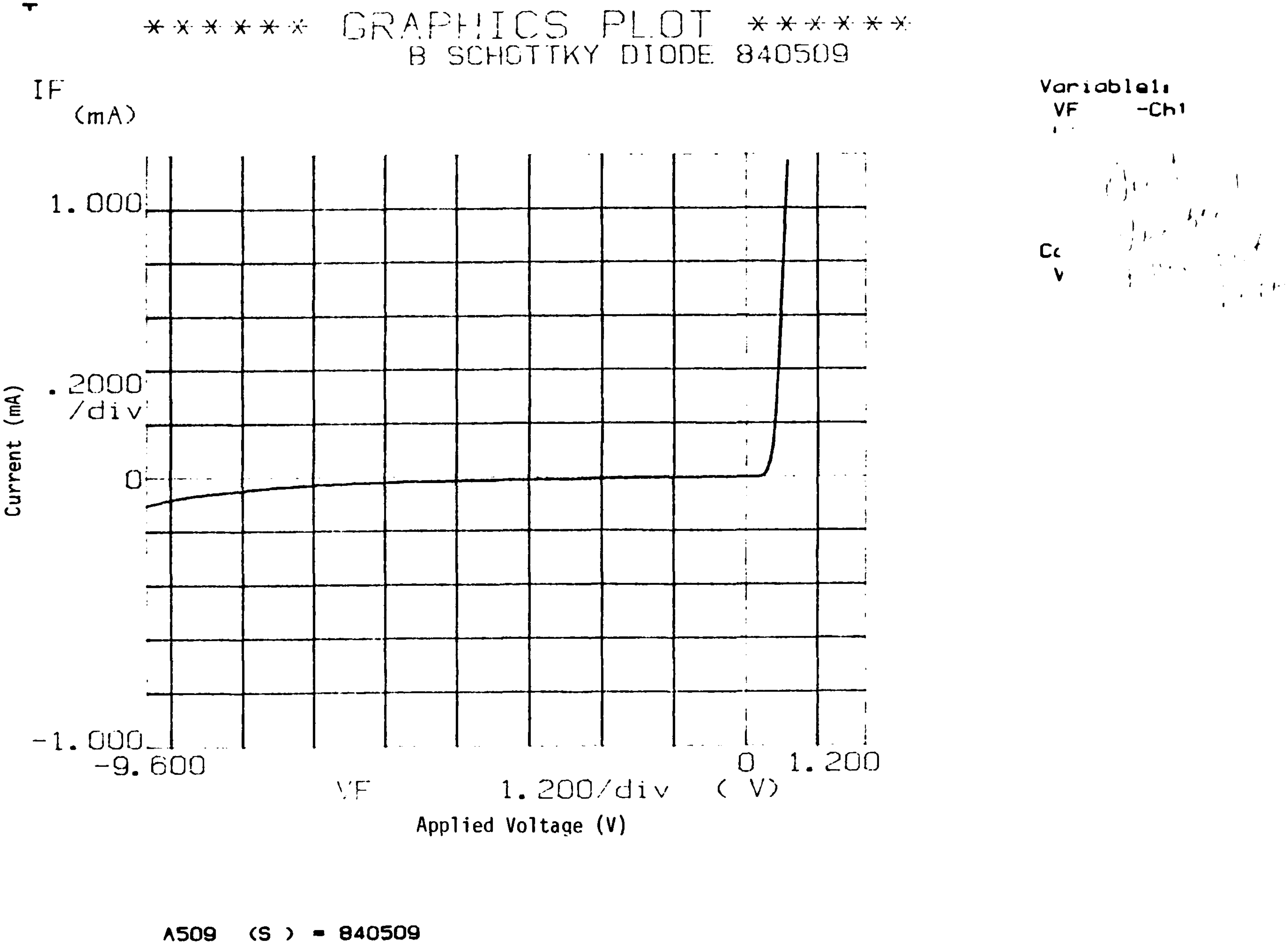

Figure 28. I-V characteristics of a back-to-back Schottky diode in 10μm thick β-SiC sample using In (ohmic) and Au (rectifying) contacts.

XI. DEVICE FABRICATION

Because of the necessity to make ohmic contacts on small dimension devices, studies of the application and formation of materials for ohmic contacts has been studied. The research for this reporting period has concentrated on the evaporation of a 97% Au/3% Ta alloy on n-type intrinsic β-SiC. The I-V characteristics for this alloy as evaporated on the aforementioned film are shown as the (a) curve in Fig. 29 which indicates that it was not ohmic in this state. However, upon heating the sample for five minutes, the ohmic characteristics improved until at 1150°C, the contact did indeed assume very good ohmic character (see curve (b) in Fig. 29).

Two of the devices which we wish to make from the SiC films are MESFETs and a mesa structure diode. To fabricate the former, 20μm, 50μm and 100μm channel length masks have been made of which the 50μm mask is shown in Fig. 30. Fabrication of this device is now underway.

Finally, Fig. 31 shows the proposed step-by-step procedure to be used in the fabrication of a p^+-n mesa structure diode.

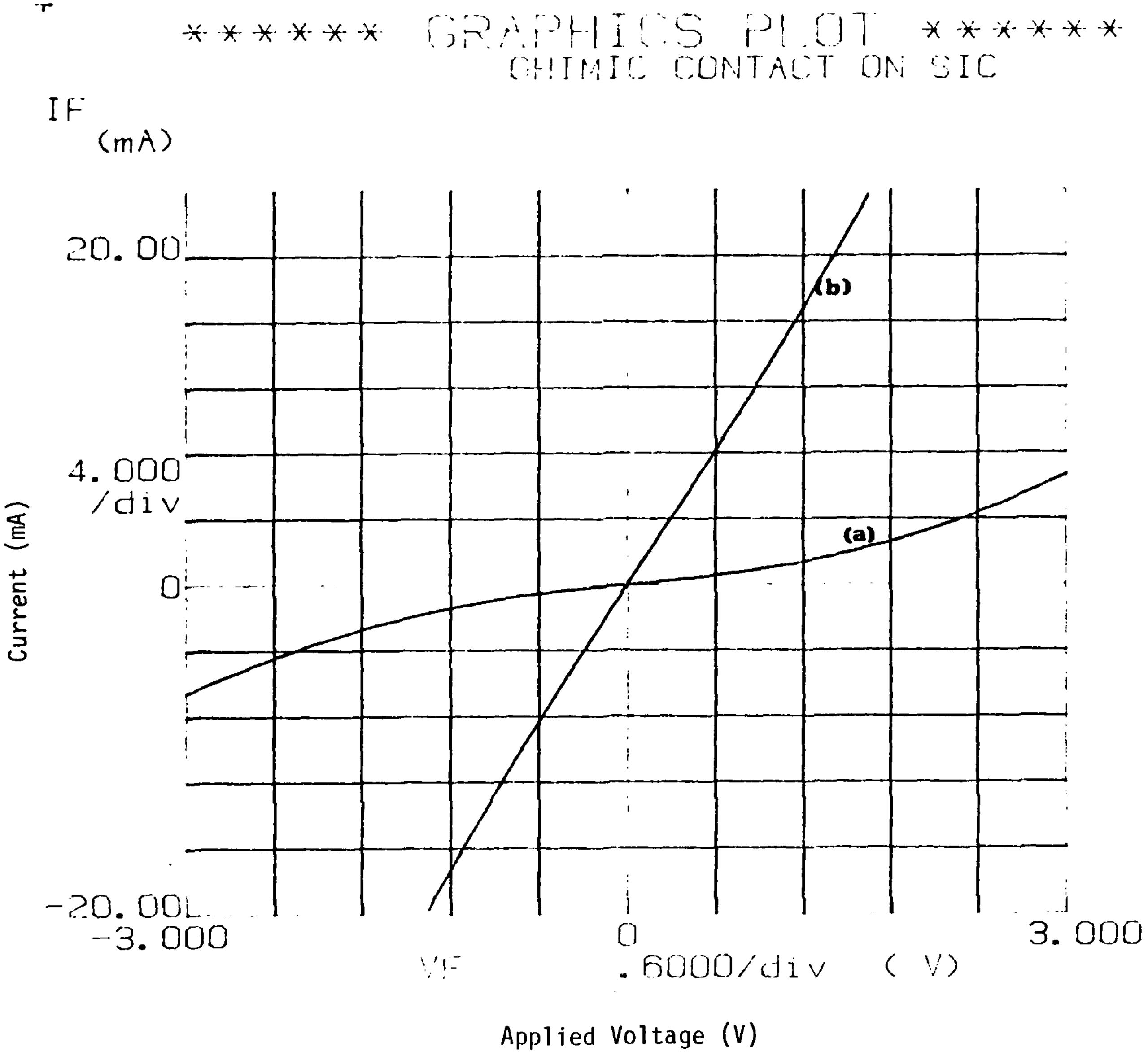

Variable1:
VF -Ch1
Linear sweep
Start -7.0000V
Stop 7.0000V
Step .0500V

Constants:
V -Ch3 .0000V

OHIMIC( ) = 2

Figure 29. I-V characteristics of an evaporated 97% Au/3% Ta film contact (a) as-evaporated, (b) after heating at 1150°C for 5 minutes.

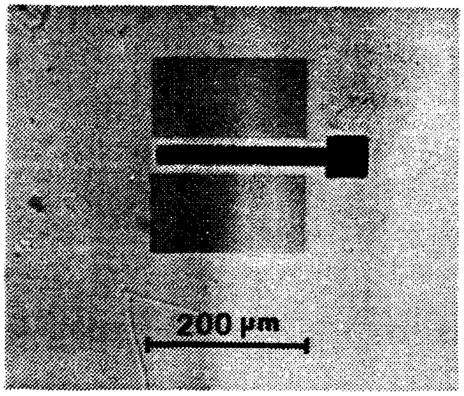

Figure 30. Fifty micron channel length mask for FET fabrication.

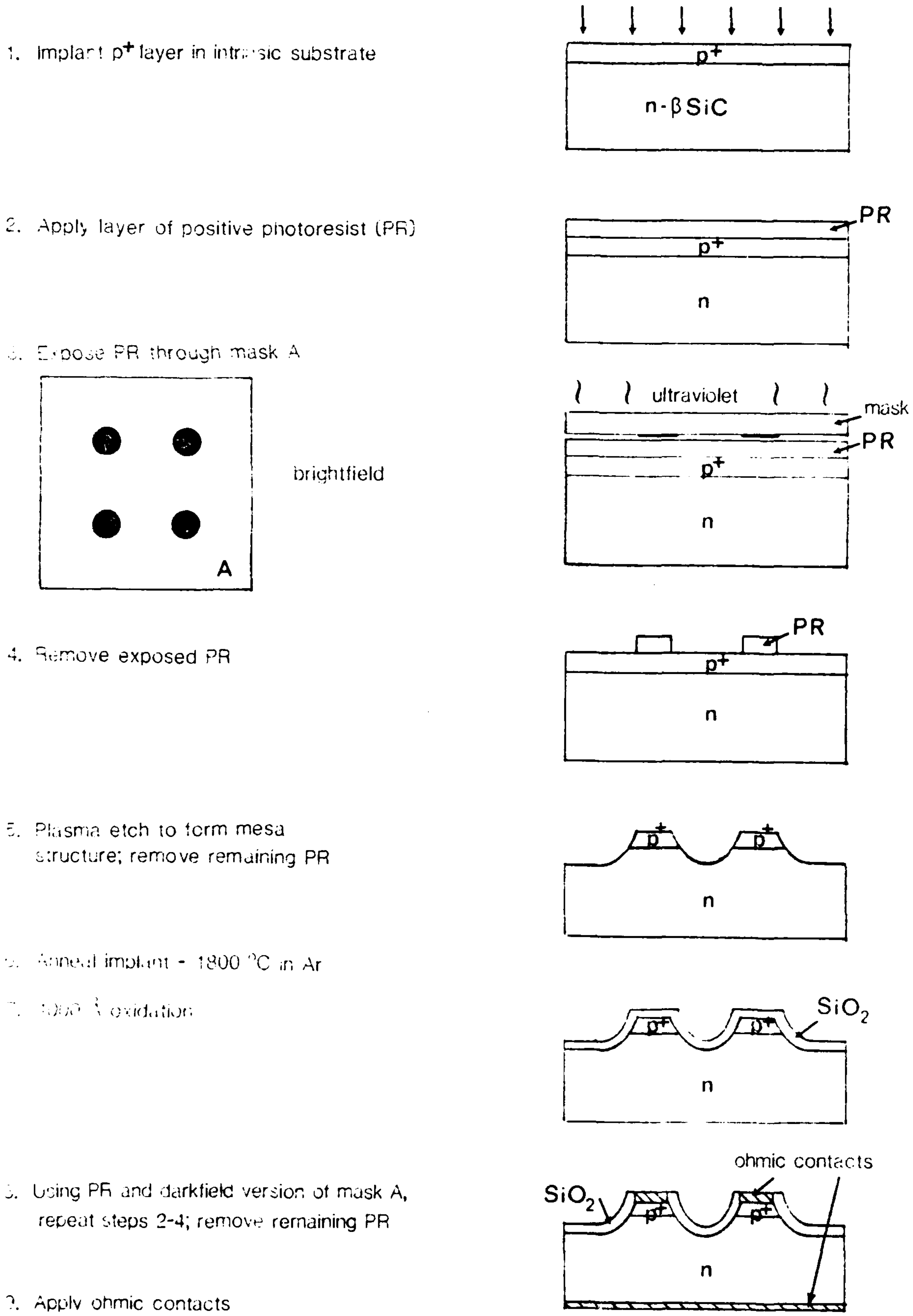

1. Implant p+ layer in intrinsic substrate
2. Apply layer of positive photoresist (PR)
3. Expose PR through mask A
4. Remove exposed PR
5. Plasma etch to form mesa structure; remove remaining PR
6. Anneal implant - 1800 °C in Ar
7. 1000 Å oxidation
8. Using PR and darkfield version of mask A, repeat steps 2-4; remove remaining PR
9. Apply ohmic contacts

Figure 31. Step wise procedure for the fabrication of a p^+-n mesa structure diode.

XII. REFERENCES

1. R. . Bartlett and R. A. Mueller, Mat. Res. Bull. 4 S341 (1969).

2. N. N. Long, D.S. Nedzvetskii, N. K. Prokofeva and M. B. Reifman, Opt. Spektosk. 29 388 (1970).

3. S. Nishino, H. Suhara and H. Matsunami, in Extended Abstracts of the 15th Conference on Solid State Devices and Materials, Tokyo, 1983, pp. 317-320.

4. W. von Muench and E. Pettenapul, J. Electrochem. Soc. 125 294 (1978).

5. W. H. Sheperd, J. Electrochem. Soc. 115 541 (1968).

6. H. Reiss, J. Chem. Phys. 21 1209 (1953).

7. P. Rai-Choudhyry and E. I. Salkovitz, J. Cryst. Growth 7 353 (1970).

8. D. R. Stull and H. Prophet, JANAF Thermochemical Tables, Second edition, NSRDS-NBS 37, National Bureau of Standards, USA (1971).

9. J. Bloem, J. Electrochem. Soc. 117 1397 (1970).

10. S. W. Pang, "Dry Etching Induced Damage in Si and GaAs," Solid State Tech. 27 249 (April 1984).

11. S. Matsui, et al., "Reactive Ion-Beam Etching of Silicon Carbide," Jap. J. of Appl. Phys., Vol. 20, No. 1, January 1981, pp. L38-L40.

12. H. Kuwabara and S. Yamada, Phys. Stat. Sol. (a) 30 739 (1975).

END

FILMED

2-85

DTIC